Passive Tracking in Heavy Clutter With Sensor Location Uncertainty

YUNFEI GUO
Hangzhou Dianzi University
Hangzhou, China

RATNASINGHAM THARMARASA
McMaster University
Hamilton, Canada

SREERAMAN RAJAN, Senior Member, IEEE
Carleton University
Ottawa, Canada

TAEK LYUL SONG, Member, IEEE
Hanyang University
Ansan, South Korea

THIA KIRUBARAJAN, Senior Member, IEEE
McMaster University
Hamilton, Canada

In order to address the problem of passive tracking from multiple asynchronous angle-only sensors with location uncertainty in heavy clutter, a new iterative maximum-likelihood probabilistic data-association algorithm is proposed in this paper. An iterative prediction–update framework is adopted in the algorithm to simultaneously estimate the target state as well as the sensor state. At the prediction stage, a deterministic sampling approach is used to adjust the measurement covariance with sensor location uncertainty. Then a two-step grid-search technique is proposed to optimize the log-likelihood ratio, combined with a gradient-based search method. At the update stage, the operational sensor states are updated with target state estimates and measurements in corresponding validation gates. The updated sensor states are used to establish a more accurate log-likelihood ratio in the next iteration, which leads to better parameter estimation. In addition, the effects of the sensor location uncertainty on the track acceptance test and the posterior Cramér–Rao lower bound are also analyzed. Simulation results show that the proposed method provides a computationally efficient way to improve track initialization performance in heavy clutter with sensor location uncertainty. The proposed work has applications in sonar tracking, geolocation, electronic support measures, and infrared search and tracking systems.

Manuscript received November 3, 2014; revised September 9, 2015; released for publication April 12, 2016.

DOI. No. 10.1109/TAES.2016.140820.

Refereeing of this contribution was handled by V. Matta.

Authors' addresses: Y. Guo, Hangzhou Dianzi University, Automation School, 1 Second Street, Xiasha, Hangzhou 310018, China; R. Tharamarasa, T. Kirubarajan, McMaster University, Electrical and Computer Engineering, 1280 Main Street West, Hamilton, Ontario L8S 4K1, Canada, E-mails: (tharman@grads.ece.mcmaster.ca, kiruba@mcmaster.ca); S. Rajan, Mackenzie 4480, Carleton University, 1125 Colonel By Drive, Ottawa, Ontario K1S 5B6, Canada, E-mail: (sreeramanr@sce.carleton.ca); T. L. Song, Hanyang University, Electronic Systems Engineering, Sa-3 Dong 1271 Sangnok-Gu, Ansan-Si, Gyeonggi-Do 426-791, South Korea, E-mail: (tsong@hanyang.ac.kr). Corresponding author is Y. Guo, E-mail: (gyf@hdu.edu.cn).

I. INTRODUCTION

Passive angle-only tracking has many applications in safety- and security-related areas (e.g., antisubmarine warfare with sonobuoys, tank self-defense with acoustic or electro-optical/infrared sensors, geolocation from an airborne platform) [3, 4]. Early research focused on ways to track targets using a single sensor or platform [9, 28]. Much work has been done to deal with the problems of nonlinearity, observability [24], and low detection probability [19, 23] in passive tracking. Advances in sensor, computer, and communication technologies have made it possible to track targets with multiple sonobuoys or electro-optical/infrared cameras [20, 25]. Compared with the single-sensor case, the multisensor application has the advantage of ensuring observability without the need for platform motion [4]. In maritime surveillance, hundreds of sonobuoys are typically deployed from a helicopter in a surveillance region to receive acoustic signals emitted from targets in a passive and asynchronous manner. All observations are then transferred to a central processing unit for formation of track estimates [25]. A similar problem is addressed in initializing tracks using unattended ground sensors or passive electro-optical/infrared sensors [3, 4].

In multiple-sensor applications, a common assumption is that the sensor location is exactly known a priori, but this is not valid unless each sensor is equipped with a GPS receiver/transmitter. In practice, sensors like sonobuoys may drift due to ocean current, and their locations may become uncertain and time varying. In fact, even the sensors' initial locations can only be assumed with uncertainty when they are dropped off from the air. Sensor location uncertainty makes angle-only estimation a challenging problem, together with nonlinearity, asynchronous reception, and measurement origin uncertainty due to false alarms and missed detections [11, 18, 22]. The performance of various tracking algorithms is investigated in [22] with real data obtained from a field of sonobuoys. The conclusion is that, without compensating for sonobuoy movement, the estimation performance degrades. A state augmentation method is presented in [25] to estimate the target state as well as the sensor state. However, additional information—namely, the bearings of sensors measured from the aircraft—is needed to calculate the sensor location. A shifted Rayleigh filter is proposed in [11] to track a nonmaneuvering target from a mobile

platform with uncertain process noise. A solution is developed in [18] for locating a moving source using time difference of arrival and frequency difference of arrival measurements in the presence of random errors in receiver locations. Both approaches need additional information and are only effective in benign environments. To account for sensor location uncertainty in heavy clutter without any additional information, two frameworks are provided in [29]. The first framework augments the state space to yield estimation results with better accuracy at the cost of additional computational complexity. The second framework, based on Taylor-series approximation, is a computationally efficient formulation where the dimensionality of the posterior Cramér–Rao lower bound (PCRLB) is fixed. For real-time sensor management in a large-scale sensor network, an approximate measurement covariance modification approach is adopted in [33, 34] to tackle sensor location uncertainty.

Since optimal tracking performance can be achieved if all sensor locations are known, our proposed work aims to estimate the sensor state and the target states simultaneously, reducing the computational complexity. In fact, the problem of tracking a target from multiple drifting sonobuoys with uncertain locations is similar to the problem of simultaneous location and mapping in robotics [2, 13]. In both cases, the objective is to estimate the states of the observer and the observed based on the noisy mapping relationship (or the measurement) between them. However, the problem tackled in this paper is more challenging: Both the observer state and the observed state are unknown; the sensors are passive and asynchronous; and the measurement origin uncertainty has to be considered. In this paper, an iterative maximum-likelihood probabilistic data-association (IML-PDA) algorithm is proposed. Similar to simultaneous location and mapping, the proposed method simultaneously estimates the target state and the sensor state. In view of the measurement origin uncertainty and asynchronous mode in our case, the proposed method deals with the state estimation problem in a batch framework.

Each iteration in IML-PDA is composed of two stages: prediction and update. At the prediction stage, all operational sensor states are predicted using their state estimates from the last iteration and their motion models. In view of additional error introduced by sensor location uncertainty, a deterministic sampling-based approach [1] is invoked to modify the measurement covariance matrix, which is then used to calculate the log-likelihood ratio (LLR). Since the LLR is a highly nonconvex function containing many local maxima and large near-zero-gradient regions [7], a rough grid-searching technique is necessary to obtain a good initial value. To reduce the computational complexity in the rough grid-searching procedure, a two-step optimization approach is proposed. It optimizes the bearing LLR with the grid-search method first to get the initial value for the position and the velocity components, and then maximizes the total LLR with the grid-search method to get the initial value for the frequency component. A gradient-based technique is then used to find the final global optimal value of all components with the total LLR.

At the update stage, all operational sensor states are updated with the estimated target state and measurements in corresponding validation gates. To avoid numerical instability in factorizing the sensor-state covariance matrix due to the sensor location uncertainty, a square-root version of the cubature Kalman filter is adopted [1]. Note that any other nonlinear update mechanism (e.g., unscented Kalman Filter [21]) can be used as well. The updated sensor states are then used to obtain a more accurate LLR in the next iterative procedure and in turn to get a more accurate target state estimation.

There are three main contributions in this paper. First, an iterative optimization framework is presented in which both the sensor state and the target state are updated. This iterative procedure helps to obtain a more accurate LLR and hence more accurate target state estimation. Second, a deterministic sampling-based modified measurement covariance technique is presented and applied to calculate the PCRLB in real time. Compared with the conventional methods, the computational complexity is linear in the number of sensors, which is vital for real-time computation in view of the ensuing optimization problem and the PCRLB computation. Third, a two-step grid-search approach, designed especially for the narrowband sonar case, is proposed in the rough grid-searching procedure to reduce its computational complexity. In addition, the effect of the sensor location uncertainty on the track acceptance test and the PCRLB are analyzed in this paper. It is demonstrated that with sensor location uncertainty, the information reduction factor (IRF) is dependent on the geometry of the target and the sensor. The IRF is time varying even if the detection probability is constant with sensor location uncertainties.

The remainder of this paper is organized as follows. In Section II, the problem and the system model are introduced. A basic framework of ML-PDA without sensor location uncertainty is summarized in Section III. In Section IV, the traditional techniques for solving the sensor location uncertainty are introduced. The proposed IML-PDA algorithm is presented in Section V. The acceptance test and the PCRLB with sensor location uncertainty are derived in Sections VI and VII, respectively. Section VIII presents the simulation results, and Section IX contains the conclusions.

II. PROBLEM FORMULATION

A. Target State Model

In passive tracking applications, the target is usually assumed to be nonmaneuvering and noise free during the surveillance period [23]. Its motion can by described by the linear dynamic system

$$X_{t,k+1} = F_k X_{t,k}, \tag{1}$$

where $X_{t,k} \in \mathcal{R}^{d_t}$ is the target state vector of dimension d_t at time k, $0 \le k \le K$. In the case of narrowband sonar, the state vector has five components $X_{t,k} = [x_{t,k}, \dot{x}_{t,k}, y_{t,k}, \dot{y}_{t,k}, f]^{\mathrm{T}}$, where $(x_{t,k}, y_{t,k})$ and $(\dot{x}_{t,k}, \dot{y}_{t,k})$ denote, respectively, its position and velocity in (x, y) coordinates at time k, and f is the constant frequency emitted by the target. Note that the algorithm designed here works equally well with the general angle-only tracking problem and with specific narrowband sonar with angle and frequency measurements. The state transition matrix $F_k = \mathrm{diag}\{F_k^*, 1\}$ is given as follows:

$$F_k^* = I_2 \otimes \begin{bmatrix} 1 & \Delta_k \\ 0 & 1 \end{bmatrix}, \tag{2}$$

where I_2 is a 2×2 identity matrix, Δ_k is the sampling interval, and $\otimes$ denotes the Kronecker product. Then the target state sequence up to and including time K can be denoted by $X_{t,0:K} = \{X_{t,k}\}_{k=0}^{K}$.

B. Sensor State Model

Assume that the fusion center receives reports from n asynchronous sensors. Each sensor is assumed to have a different initial measurement time but the same sampling interval. In view of the fact that there is no interaction between different sensors in our proposed method, the measurement time of the ith sensor is denoted as k instead of $k(i)$ for simplicity.

The sensors' locations are uncertain due to external forces, such as wind and ocean current. For the ith sensor, $1 \le i \le n$, its uncertain motion is usually modeled by a random walk [29, 34]. A more complicated sensor dynamic model can be used if a priori knowledge about it is known [22, 25]. That is,

$$X_{s,k+1}^i = F_k^* X_{s,k}^i + v_{s,k}^i, \tag{3}$$

where $X_{s,k}^i \in \mathcal{R}^{d_s}$ is the sensor state vector of dimension d_s at time k and has four components $X_{s,k}^i = [x_{s,k}^i, \dot{x}_{s,k}^i, y_{s,k}^i, \dot{y}_{s,k}^i]^{\mathrm{T}}$. Assume that the sensors' velocities are much less than the target velocity and can be omitted in view of the Doppler shift frequency (DSF); then only their position components in the state must be considered—i.e., $X_{s,k}^i = [x_{s,k}^i, y_{s,k}^i]^{\mathrm{T}}$ [10]. The sensor process noise $v_{s,k}^i$ is assumed to be zero-mean white Gaussian noise with covariance $Q_{s,k}^i$. For simplicity, assume that the process noises of different sensors are mutually independent. Assuming that the target and the sensors are in the same environment and are affected by almost the same current, the process noise in the target model is negligible, since the target—e.g., a ship—is usually much heavier than the drifting sensors, e.g., sonobuoys.

The ith sensor's state sequence up to and including time K can be denoted by $X_{s,0:K}^i = \{X_{s,k}^i\}_{k=0}^{K}$, and the state sequence of the entire sensor set up to and including time K can be denoted by $X_{s,0:K} = \{X_{s,0:K}^i\}_{i=1}^{n}$. In the proposed application, each sensor is deployed from a moving platform, e.g., a helicopter, and the initial sensor location is assumed to be $X_{s,0}^i \sim N(\bar{X}_{s,0}^i, P_{s,0}^i)$, $i = 1, \ldots, n$, where $\bar{X}_{s,0}^i$ is the deployment mean and $P_{s,0}^i$ is the corresponding covariance.

C. Measurement Model

Assume that there are m_k^i measurements received by the ith sensor at time k, each measurement either originated from the target or a false alarm. Denote the jth measurement as $z_{k,j}^i \in \mathcal{R}^{d_z}$, $j = 1, \ldots, m_k^i$, where d_z is the measurement dimension. A general measurement model in clutter is given by [30]

$$z_{k,j}^i = \begin{cases} h_k^i\left(X_{t,k}, X_{s,k}^i\right) + w_{k,j}^i & \text{from target} \\ u_{k,j}^i & \text{false alarm} \end{cases}, \tag{4}$$

$j = 1, \ldots, m_k^i$. For narrowband sonar, the sensor can get both the bearing and DSF information, i.e., $z_{k,j}^i = [\theta_{k,j}^i, \gamma_{k,j}^i]^{\mathrm{T}}$. If the jth measurement is target originated, it is assumed to be disturbed by a zero-mean white Gaussian noise $w_{k,j}^i$ with constant covariance $R = \mathrm{diag}\{\sigma_\theta^2, \sigma_\gamma^2\}$, where σ_θ and σ_γ are the standard deviations of the bearing and DSF measurements, respectively. Otherwise, the measurement is assumed to be a uniform distribution in the surveillance region Ω, with $u_{k,j}^i = [u_{\theta,k,j}^i, u_{\gamma,k,j}^i]^{\mathrm{T}}$, $u_{\theta,k,j}^i \sim U[\Theta_1, \Theta_2]$, and $u_{\gamma,k,j}^i \sim U[\Gamma_1, \Gamma_2]$.

For the target-originated measurement, the measurement function $h_k^i = [h_{\theta,k}^i, h_{\gamma,k}^i]^{\mathrm{T}}$ is given as follows [10]:

$$h_{\theta,k}^i \triangleq h_{\theta,k}^i\left(X_{t,k}, X_{s,k}^i\right) = \arctan\frac{x_{t,k} - x_{s,k}^i}{y_{t,k} - y_{s,k}^i} \tag{5}$$

$$\begin{aligned} h_{\gamma,k}^i &\triangleq h_{\gamma,k}^i\left(X_{t,k}, X_{s,k}^i\right) \\ &= f \cdot \left(1 + \left(\dot{x}_{s,k}^i - \dot{x}_{t,k}\right)\Gamma_{k,1}^i + \left(\dot{y}_{s,k}^i - \dot{y}_{t,k}\right)\Gamma_{k,2}^i\right), \end{aligned} \tag{6}$$

where $\Gamma_{k,1}^i = (x_{t,k} - x_{s,k}^i)/cr_k^i$, $\Gamma_{k,2}^i = (y_{t,k} - y_{s,k}^i)/cr_k^i$, $r_k^i = \sqrt{(x_{t,k} - x_{s,k}^i)^2 + (y_{t,k} - y_{s,k}^i)^2}$, and c is the signal speed in medium. Assume that sensor's velocity is small compared with the target's velocity; then a simpler version of the DSF is given as follows:

$$h_{\gamma,k}^i = f \cdot \left(1 - \dot{x}_{t,k}\Gamma_{k,1}^i - \dot{y}_{t,k}\Gamma_{k,2}^i\right). \tag{7}$$

Note that the calculation of the DSF in (7) involves only the sensor location; that will be used as the DSF model in this paper. The false alarms are uniformly distributed in the surveillance region, and their cardinality is Poisson distributed with parameter λV, i.e.,

$$u_f\left(m_k^i\right) = \frac{(\lambda V)^{m_k^i}\exp(-\lambda V)}{m_k^i!}, \tag{8}$$

where $V = (\Theta_2 - \Theta_1)(\Gamma_2 - \Gamma_1)$ is the volume of Ω. Also, $\lambda = P_{\mathrm{FA}}/V_{\mathrm{C}}$ is the expected number of false alarms per unit volume and P_{FA} is the probability of false alarms. If a Swerling I model [23] is used for detection and the

signal-to-noise ratio (SNR) in a resolution cell is denoted as $\mathrm{SNR_C}$, the following relationship can be achieved [16]:

$$P_{\mathrm{FA}} = (P_{\mathrm{D}})^{1+\mathrm{SNR_C}}, \tag{9}$$

where P_{D} is the probability of detection. It is assumed that the SNR is constant during the measurement period, but a more complicated SNR model can be found in [29]. In the foregoing, V_{C} is the resolution cell volume of the signal processor. For narrowband sonar, $V_{\mathrm{C}} = C_\theta C_\gamma$, where C_θ is the bearing cell size and C_γ is the frequency cell size. Assuming uniform distribution in a cell, the bearing and DSF measurements' standard deviations are given by $\sigma_\theta = C_\theta/\sqrt{12}$ and $\sigma_\gamma = C_\gamma/\sqrt{12}$ [23].

The measurement set of the ith sensor at time k is denoted as $Z_k^i = \{z_{k,j}^i\}_{j=1}^{m_k^i}$, and the temporal measurement set of the ith sensor up to and including time K is denoted as $Z_{1:K}^i \triangleq \{z_k^i\}_{k=1}^K$. The spatial measurement set of the fusion center is denoted as $Z_{1:K} = \{Z_{1:K}^i\}_{i=1}^n$.

The objective of our problem is to estimate the target trajectory $X_{t,0:K}$ conditioned on the cumulative measurement set $Z_{1:K}$ from multiple asynchronous sensors $X_{s,0:K}$ with location uncertainty.

III. BASIC ML-PDA FRAMEWORK

Before introducing the basic framework of ML-PDA, several assumptions about the statistical characteristics the measurements are made [19, 23]:

1) The target-originated measurement at a measurement time is received by the sensor at most once with a certain detection probability and is corrupted with additive zero-mean Gaussian noise.
2) The measurements at two different measurement times of each sensor are conditionally independent.
3) The false alarms are distributed uniformly in the surveillance region.
4) The number of false alarms is Poisson distributed with parameter λV.
5) The measurements from different sensors are conditionally independent.

Under these assumptions, the following mutually exclusive and exhaustive events of the ith sensor can be obtained at time k: Either all m_k^i measurements are false alarms or there is one true observation of the target and $m_k^i - 1$ false alarms. Using the total probability theorem, the prior probability $p(m_k^i)$ that there are m_k^i observations at time k is given by

$$p\left(m_k^i\right) = (1 - P_{\mathrm{D}})\, u_f\left(m_k^i\right) + P_{\mathrm{D}} u_f\left(m_k^i - 1\right). \tag{10}$$

The probability that one measurement is target originated is then as follows:

$$\varepsilon\left(m_k^i\right) = \frac{P_{\mathrm{D}}}{p\left(m_k^i\right)} u_f\left(m_k^i - 1\right). \tag{11}$$

Then the probability density function (pdf) of the set of measurements Z_k^i given $(X_{t,k}, X_{s,k}^i, m_k^i)$ is given by

$$p\left(Z_k^i \,|X_{t,k}, X_{s,k}^i, m_k^i\right) = \left[1 - \varepsilon\left(m_k^i\right) + \frac{\varepsilon\left(m_k^i\right)}{m_k^i} \sum_{j=1}^{m_k^i} \frac{p_1\left(z_{k,j}^i\right)}{p_0\left(z_{k,j}^i\right)}\right] \left[\prod_{j=1}^{m_k^i} p_0\left(z_{k,j}^i\right)\right], \tag{12}$$

where p_1 is the pdf of a true detection and p_0 is the false-alarm pdf. Using the measurement model in Section II.C, the following can be obtained:

$$p_1\left(z_{k,j}^i\right) = \frac{1}{2\pi\sigma_\theta\sigma_\gamma} \exp\left(-\frac{1}{2}\left(\frac{\left(\theta_{k,j}^i - h_{\theta,k}^i\right)^2}{\sigma_\theta^2} + \frac{\left(\gamma_{k,j}^i - h_{\gamma,k}^i\right)^2}{\sigma_\gamma^2}\right)\right) \tag{13}$$

$$p_0\left(z_{k,j}^i\right) = 1/V. \tag{14}$$

Then the likelihood of the set of measurements Z_k^i given $(X_{t,k}, X_{s,k}^i)$ can be obtained by substituting (10)–(12) and (14) as

$$\begin{aligned} p\left(Z_k^i \,|X_{t,k}, X_{s,k}^i\right) &= p\left(m_k^i\right) p\left(Z_k^i \,|X_{t,k}, X_{s,k}^i, m_k^i\right) \\ &= \frac{(1 - P_{\mathrm{D}})\, u_f\left(m_k^i\right)}{V^{m_k^i}} + \frac{P_{\mathrm{D}} u_f\left(m_k^i - 1\right)}{m_k^i V^{m_k^i - 1}} \sum_{j=1}^{m_k^i} p_1\left(z_{k,j}^i\right). \end{aligned} \tag{15}$$

Dividing (15) by the likelihood of all false alarms $u_f(m_k^i)/V^{m_k^i}$, the dimensionless likelihood ratio of the ith sensor at time k is given by

$$\Phi_k^i\left(Z_k^i \,|X_{t,k}, X_{s,k}^i\right) = (1 - P_{\mathrm{D}}) + \frac{P_{\mathrm{D}}}{\lambda} \sum_{j=1}^{m_k^i} p_1\left(z_{k,j}^i\right). \tag{16}$$

Alternatively, its LLR can be defined as

$$\phi_k^i\left(Z_k^i \,|X_{t,k}, X_{s,k}^i\right) = \ln\left[(1 - P_{\mathrm{D}}) + \frac{P_{\mathrm{D}}}{\lambda} \sum_{j=1}^{m_k^i} p_1\left(z_{k,j}^i\right)\right]. \tag{17}$$

The likelihood function of the temporal measurement set of the ith sensor up to and including time K can be written as

$$p\left(Z_{1:K}^i \,|X_{t,0:K}, X_{s,0:K}^i\right) = \prod_{k=1}^{K} p\left(Z_k^i \,|X_{t,k}, X_{s,k}^i\right). \tag{18}$$

The dimensionless likelihood ratio and its log version for the temporal measurement set of the ith sensor are given

by

$$\Phi^i_{1:K}\left(Z^i_{1:K}\,\middle|\,X_{t,0:K},\,X^i_{s,0:K}\right)=\prod_{k=1}^{K}\Phi^i_k\left(Z^i_k\,\middle|\,X_{t,k},\,X^i_{s,k}\right) \tag{19}$$

$$\phi^i_{1:K}\left(Z^i_{1:K}\,\middle|\,X_{t,0:K},\,X^i_{s,0:K}\right)=\sum_{k=1}^{K}\phi^i_k\left(Z^i_k\,\middle|\,X_{t,k},\,X^i_{s,k}\right). \tag{20}$$

The likelihood function of the spatial measurement set of the fusion center can be written as

$$\begin{aligned}&p\left(Z_{1:K}\,\middle|\,X_{t,0:K},\,X_{s,0:K}\right)\\&\quad=\prod_{i=1}^{n}p\left(Z^i_{1:K}\,\middle|\,X_{t,0:K},\,X^i_{s,0:K}\right)\\&\quad=\prod_{i=1}^{n}\prod_{k=1}^{K}p\left(Z^i_k\,\middle|\,X_{t,k},\,X^i_{s,k}\right).\end{aligned} \tag{21}$$

The dimensionless likelihood ratio and its log version for the spatial measurement set of the fusion center are given by

$$\Phi_{1:K}\left(Z_{1:K}\,\middle|\,X_{t,0:K},\,X_{s,0:K}\right)=\prod_{i=1}^{n}\prod_{k=1}^{K}\Phi^i_k\left(Z^i_k\,\middle|\,X_{t,k},\,X^i_{s,k}\right) \tag{22}$$

$$\phi_{1:K}\left(Z_{1:K}\,\middle|\,X_{t,0:K},\,X_{s,0:K}\right)=\sum_{i=1}^{n}\sum_{k=1}^{K}\phi^i_k\left(Z^i_k\,\middle|\,X_{t,k},\,X^i_{s,k}\right). \tag{23}$$

The ML estimate is obtained by finding the target state sequence $\hat{X}_{t,0:K}$ and the sensors state sequence $\hat{X}_{s,0:K}$ that maximize the total LLR (23) or minimize its negative version. That is,

$$\left[\hat{X}_{t,0:K},\,\hat{X}_{s,0:K}\right]=\underset{X_{t,0:K},\,X_{s,0:K}}{\operatorname{argmax}}\left[\phi_{1:K}\left(Z_{1:K}\,\middle|\,X_{t,0:K},\,X_{s,0:K}\right)\right]. \tag{24}$$

If the sensor location is determined and known in (24), the following conventional ML-PDA problem can be obtained:

$$\hat{X}_{t,0:K}=\underset{X_{t,0:K}}{\operatorname{argmax}}\left[\phi_{1:K}\left(Z_{1:K}\,\middle|\,X_{t,0:K}\right)\right]. \tag{25}$$

Furthermore, under the assumption that the target is nonmaneuvering during the surveillance period, the state estimation problem reduces to a parameter estimation problem [4], i.e.,

$$\hat{X}_{t,0}=\underset{X_{t,0}}{\operatorname{argmax}}\left[\phi_{1:K}\left(Z_{1:K}\,\middle|\,X_{t,0}\right)\right]. \tag{26}$$

In a sliding-window-based ML-PDA algorithm, designed for use in real-time applications, a set of the K most recent data frames is used to compute the initial state at the beginning of the sliding window.

IV. PREVIOUS WORK ON SENSOR LOCATION UNCERTAINTY

In traditional angle-only tracking, the sensor location is usually assumed to be known, which is reasonable for an observing platform equipped with a GPS transmitter/receiver. However, the sensors deployed in real angle-only tracking applications (e.g., sonobuoys, unattended ground sensors) are usually not equipped with GPS sensors due to cost. They are usually deployed from a mobile platform with an uncertain initial position and followed by an uncertain drifting motion due to the environment [25]. In addition, the sensor location uncertainty will increase with time after deployment. Real trial data were used in [22] to show that the tracking performance will degrade rapidly unless the effects of sensor location uncertainty are considered. In this section, a brief introduction to some common techniques will be provided.

There are two major methods to deal with sensor location uncertainty. The first approach is called state augmentation (SA) [25, 29], in which the state vector is augmented to include the states of the operational sensor results in better performance at the cost of more computational complexity. The second approach is based on modifying the measurement covariance to incorporate the sensor location uncertainties [29].

A. State Augmentation

The idea behind this method is to include the sensor state in the system state along with the target state [29]. The system state is defined as $X_k \triangleq [X_{t,k},\,X^1_{s,k},\ldots,X^n_{s,k}]^{\mathrm{T}}$, of dimension (d_t+nd_s), and its dynamic equation can be rewritten as

$$X_{k+1}=\mathbf{F}_kX_k+v_k. \tag{27}$$

The system transition matrix is a block diagonal matrix $\mathbf{F}_k=\operatorname{diag}\{F_k,\,F^*_k,\ldots,F^*_k\}$ of dimension $(d_t+nd_s)\times(d_t+nd_s)$. System process noise $\{v_k\}$ is a zero-mean Gaussian white-noise sequence with a block diagonal covariance matrix $Q_k=\operatorname{diag}\{0,\,Q^1_{s,k},\ldots,Q^n_{s,k}\}$ of the same dimension as $\mathbf{F}_k$.

The SA method can obtain an optimal estimate at the cost of added computational complexity [29]. In a Bayesian approach, the SA method can be used to estimate the target state as well as the sensor state during filtering [29]. In a non-Bayesian approach, if the true sensor location is unknown but deterministic or nearly deterministic, the tracking problem with the SA method becomes one of solving a high-dimensional optimization problem of dimension (d_t+nd_s). In large-scale problems, the SA method is computationally expensive, and real-time performance cannot be guaranteed.

B. Taylor-Series-Based Measurement Covariance Modification

As mentioned earlier, the initial sensor location's distribution is denoted as $X^i_{s,0}\sim N(\bar{X}^i_{s,0},\,P^i_{s,0})$,

$i = 1, \ldots, n$, and the sensor motion is described by (3) with known process noise $v^i_{s,k} \sim N(0, Q^i_{s,k})$. Let the initial sensor state estimate $\hat{X}^i_{s,0}$ take value at $\bar{X}^i_{s,0}$ and assume that the sensor state at time $k-1$ is estimated as $X^i_{s,k-1} \sim N(\hat{X}^i_{s,k-1}, P^i_{s,k-1})$; the following formulas can then be obtained from (3):

$$\hat{X}^i_{s,k} = \hat{X}^i_{s,k|k-1} = F^*_{k-1}\hat{X}^i_{s,k-1} \tag{28}$$

$$P^i_{s,k} = P^i_{s,k|k-1} = F^*_{k-1}P^i_{s,k-1}\left(F^*_{k-1}\right)^{\mathrm{T}} + Q^i_{s,k-1}. \tag{29}$$

Note that the sensor state estimate here takes value of its prediction. Assuming that the jth measurement is generated from the target, the following can be obtained from (4):

$$z^i_{k,j} = h^i_k\left(X_{t,k}, X^i_{s,k}\right) + w^i_{k,j}, \tag{30}$$

where $w^i_{k,j}$ is the zero-mean Gaussian measurement noise with covariance R. The idea behind this method is to modify the measurement covariance matrix R in order to incorporate sensor location uncertainty. Using a first-order Taylor-series approximation, the measurement equation is expanded about the sensor state estimate as follows:

$$z^i_{k,j} \approx h^i_k\left(X_{t,k}, \hat{X}^i_{s,k}\right) + H^i_k \cdot \left(X^i_{s,k} - \hat{X}^i_{s,k}\right) + w^i_{k,j}, \tag{31}$$

where $H^i_k = \nabla_{X^i_{s,k}} h^i_k(X_{t,k}, X^i_{s,k})|_{X^i_{s,k}=\hat{X}^i_{s,k}}$ is the Jacobian matrix of the measurement model with respect to the sensor state. Then (31) can be written approximately as

$$z^i_{k,j} \approx \hat{z}^i_{k,j} = h^i_k\left(X_{t,k}, \hat{X}^i_{s,k}\right) + v^i_{k,j}, \tag{32}$$

where $v^i_{k,j} \sim N(0, \hat{R}^i_k)$. The modified measurement covariance $\hat{R}^i_k$ is given by

$$\hat{R}^i_k = \hat{R}^i_k\left(X_{t,k}, \hat{X}^i_{s,k}, R\right) = H^i_k P^i_{s,k}\left(H^i_k\right)^{\mathrm{T}} + R. \tag{33}$$

Furthermore, the measurement information matrix in the PCRLB is given by

$$[J_Z(k)]_{ab} \approx \sum_{i=1}^{n} E\left\{K_1(\cdot)\left[\frac{\partial \hat{R}^i_k(\cdot)}{\partial X^a_{t,k}}\frac{\partial \hat{R}^i_k(\cdot)}{\partial X^b_{t,k}}\right] + K_2(\cdot)\left[\frac{\partial h^i_k(\cdot)}{\partial X^a_{t,k}}\frac{\partial h^i_k(\cdot)}{\partial X^b_{t,k}}\right]\right\}, \tag{34}$$

where $K_1(\cdot)$ and $K_2(\cdot)$ are defined in the appendix of [29] and could be determined using Monte Carlo integration. Also, $X^a_{t,k}$ and $X^b_{t,k}$ are the ath and bth components of the target state. Then the modified measurement covariance matrix can be obtained by an appropriate transformation.

The Taylor-series-based measurement covariance modification method to handle the sensor location uncertainty is similar to the extended Kalman filter to deal with the nonlinear filtering problem with state uncertainty. Compared with the SA method, the primary advantage of this method is that the dimension of the approximate PCRLB is always equal to the dimension of the target state, and more importantly, it does not increase as the number of operational sensors increases [29]. However, the additional computational load of calculating $K_1(\cdot)$ and $K_2(\cdot)$ in this derivation is very high even for the monostatic case. For real-time PCRLB calculation, an approximate derivation for the PCRLB by replacing R with $\hat{R}^i_k$, without taking into account the effect of sensor location uncertainty on the IRF, was proposed in [34]. Additionally, this method has limited capability to deal with strong nonlinearities, since it is based on linearization [12]. This will decrease the accuracy of the approximate measurement (32) and hence degrade tracking performance. Meanwhile, we have to take into consideration possible numerical instabilities when calculating the Jacobian matrix. In the next section, a new method is proposed to handle sensor location uncertainty in track initialization. The proposed method yields a more reliable measurement covariance and facilitates efficient calculation of the LLR. Also, a more accurate PCRLB is calculated in real time.

V. IML-PDA ALGORITHM

In this section, an iterative ML-PDA-based algorithm is presented to deal with sensor location uncertainty in heavy clutter. The basic idea behind IML-PDA is to simultaneously estimate the target and sensor states in an iterative manner. A batch of K frames is used for track initialization or track maintenance in a sliding-window manner. In each iteration, the same measurement set is used, but the updated sensor state sequence constructs an updated LLR and hence yields a more accurate track estimate. Each iteration is composed of two stages: prediction and update. At the prediction stage, the sensor state is predicted by its estimated state from the last iteration, while a deterministic sampling technique is used to modify the measurement covariance. Then the target state is estimated by finding the global maximum of the LLR. Because the LLR is calculated with the sensors' estimated location and not the true location, the global optimum of the LLR does not yield the true target state. This is in contrast with the conventional passive tracking problem, where the sensor location is exactly known. At the update stage, the sensors' states are updated by the estimated target state with measurements in corresponding validation gates. The updated sensor states are then used to obtain a more accurate LLR in the next iteration, which helps to find a more accurate target state estimate. This iterative procedure is terminated based on a given maximum iterative number $I_{\max}$ or convergence. Fig. 1 illustrates the block diagram of the IML-PDA.

For iterative initialization, in the first iteration the ith sensor's initial state is given by its deployment mean and corresponding covariance, $\hat{X}^{i,(1)}_{s,0} = \bar{X}^i_{s,0}$ and $P^{i,(1)}_{s,0} = P^i_{s,0}$, respectively. In the pth iteration ($1 < p \le I_{\max}$), the ith sensor's initial state and covariance are given by the estimated value and the corresponding covariance in the last iteration, $\hat{X}^{i,(p)}_{s,0} = \hat{X}^{i,(p-1)}_{s,0}$ and $P^{i,(p)}_{s,0} = P^{i,(p-1)}_{s,0}$, respectively. For brevity, the iteration index is omitted in the following.

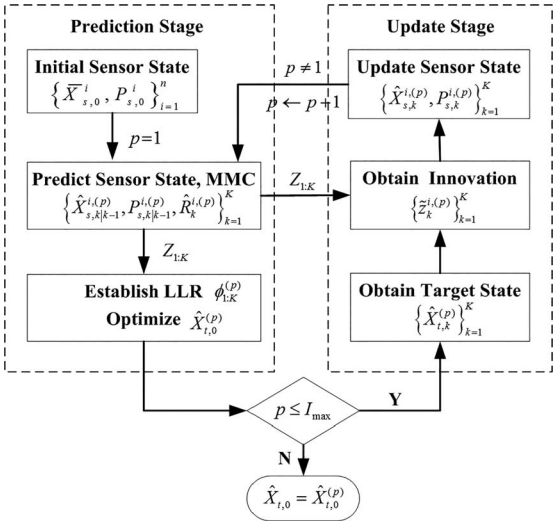

Fig. 1. Block diagram of IML-PDA.

A. Prediction Stage

1) *Deterministic Sampling-Based Modified Measurement Covariance (DS-MMC)*: There are several deterministic sampling methods to improve nonlinear filtering, including the unscented Kalman filter [21] and the cubature Kalman filter (CKF) [1]. Compared with the linearization method (extended Kalman filter) and the random sampling method (particle filter) [12], the deterministic sampling methods can yield more accurate estimation results with less computational complexity under the Gaussian assumption. In this paper, the CKF is used to deal with sensor location uncertainty; however, other techniques can be used equally well.

Assume that the estimated state's mean and covariance of the ith sensor at time $k-1$ are $\hat{X}^i_{s,k-1}$ and $P^i_{s,k-1}$, respectively. Since the sensor state model (3) is linear and Gaussian, both the predictive state $\hat{X}^i_{s,k|k-1}$ and the corresponding covariance $P^i_{s,k|k-1}$ can be obtained directly by (28) and (29). Factorize the prediction covariance matrix as

$$P^i_{s,k|k-1} = S^i_{s,k|k-1}\left(S^i_{s,k|k-1}\right)^{\mathrm{T}}. \tag{35}$$

Evaluate the cubature points of the sensor state as

$$X^i_{s,k|k-1,\eta} = S^i_{s,k|k-1}\,\xi_\eta + \hat{X}^i_{s,k|k-1}, \tag{36}$$

$\eta = 1, \ldots, 2d_s$, where $\{\xi_\eta, \omega_\eta\}_{\eta=1}^{2d_s}$ is the third-degree spherical-radial cubature weighted point set [1]. Then

$$\xi_\eta = \sqrt{d_s}[1]_\eta, \quad \omega_\eta = 1/2d_s, \tag{37}$$

where $[1]_\eta$ is the ηth component of a complete fully symmetric set of points that can be obtained by permuting and changing the sign of the generator in all possible ways. For the two-dimensional case, $[1] \in \mathcal{R}^2$ represents the following set of points:

$$\left\{\begin{pmatrix}1\\0\end{pmatrix}, \begin{pmatrix}0\\1\end{pmatrix}, \begin{pmatrix}-1\\0\end{pmatrix}, \begin{pmatrix}0\\-1\end{pmatrix}\right\}.$$

Given a target state value $X_{t,k}$ at time k, evaluate the predictive cubature points of the target-originated measurement $z^i_{k|k-1,\eta}$ as follows:

$$z^i_{k|k-1,\eta} = h^i_k\left(X_{t,k}, X^i_{s,k|k-1,\eta}\right). \tag{38}$$

The predicted measurement is estimated as follows:

$$\hat{z}^i_{k|k-1} = \sum_{\eta=1}^{2d_s} \omega_\eta z^i_{k|k-1,\eta}. \tag{39}$$

Then the MMC is given by

$$\hat{R}^i_k = \sum_{\eta=1}^{2d_s} \omega_\eta z^i_{k|k-1,\eta}\left(z^i_{k|k-1,\eta}\right)^{\mathrm{T}} - z^i_{k|k-1}\left(z^i_{k|k-1}\right)^{\mathrm{T}} + R. \tag{40}$$

Note that due to the sensor location uncertainty, the MMC is no longer a constant matrix but depends on the current target state as well as the sensor location covariance. Furthermore, this time-varying characteristic of the MMC makes the validation gate and the LLR time varying too. The corresponding modified validation gate and its volume are defined as

$$\hat{\Omega}^i_{g,k} = \left\{z^i_{k,j}:\left(z^i_{k,j} - \hat{z}^i_{k|k-1}\right)^{\mathrm{T}}\left(\hat{R}^i_k\right)^{-1}\left(z^i_{k,j} - \hat{z}^i_{k|k-1}\right) \le g^2\right\} \tag{41}$$

$$\hat{V}^i_{g,k} = \pi\hat{\sigma}^i_{\theta,k}\hat{\sigma}^i_{\gamma,k}g^2, \tag{42}$$

where $\hat{\sigma}^i_{\theta,k}$ and $\hat{\sigma}^i_{\gamma,k}$ take the roots of the eigenvalues of $\hat{R}^i_k$. Then a modified LLR can be obtained as follows:

$$\begin{aligned}\phi_{1:K}\left(\hat{Z}_{1:K}\,|X_{t,0}\right) &= \sum_{i=1}^{n}\sum_{k=1}^{K}\phi^i_k\left(\hat{Z}^i_k\,|X_{t,0}\right)\\ &= \sum_{i=1}^{n}\sum_{k=1}^{K}\ln\left[(1-P_{\mathrm{D}}) + \frac{P_{\mathrm{D}}}{\lambda}\sum_{j=1}^{m^i_k}p_1\left(\hat{z}^i_{k,j}\right)\right]\end{aligned} \tag{43}$$

$$p_1\left(\hat{z}^i_{k,j}\right) = \frac{1}{2\pi\hat{\sigma}^i_{\theta,k}\hat{\sigma}^i_{\gamma,k}}\exp\left(-\frac{1}{2}\left(\frac{\left(\theta^i_{k,j} - \hat{\theta}^i_{k|k-1}\right)^2}{\left(\hat{\sigma}^i_{\theta,k}\right)^2} + \frac{\left(\gamma^i_{k,j} - \hat{\gamma}^i_{k|k-1}\right)^2}{\left(\hat{\sigma}^i_{\gamma,k}\right)^2}\right)\right). \tag{44}$$

The deterministic sampling-based MMC method is derivative free. Its computational complexity, denoted as $O(2d_sn)$, increases linearly with the number of operational sensors. Meanwhile, the method can yield a more accurate estimate of the predicted measurement (39) and its covariance (40) based on the deterministic sampling technique.

2) *Two-Step Grid Search*: The LLR obtained from (43) is a highly nonconvex function that contains many local maxima and large near-zero-gradient regions [7]. There is no technique that can find the global maximum of

an arbitrary nonconvex objective function in polynomial time [7]. Three major techniques are presented to get a good initial estimate. The first is multipass grid search [23], which uses a scaling factor to artificially enlarge the region influenced by detections in the parameter space and to smooth the LLR surface. The second is genetic algorithm search [17], which uses a rule set based on biological evolutionary development. The third is the directed subspace search [7] for a grid-based method, which reduces the parameter space with measurement data to lower the computational complexity. The directed subspace search method is especially efficient in active tracking applications to map bearing and range measurements to Cartesian states.

To reduce computational complexity, a two-step rough grid-searching method is proposed in this paper. The essence of this method is to get the initial target state estimate in two steps. First, maximize the bearing LLR with the grid-search method to get the position and velocity components of the initial estimate. Second, based on the position and velocity components' initial values, optimize the total LLR with the grid-search method to get the frequency component's initial estimate. These initial values are then used to optimize the total LLR by a gradient-based method. The two-step rough grid-search technique is designed especially for narrowband passive sonar, where both the bearing measurement and the DSF measurement are available. The two-step rough grid-based search decreases the computational complexity by an order of magnitude compared to the standard single-step approach.

Assume that the DSF measurements are not available first and let $X_{t,0}^{1:4} \triangleq [x_{t,0}, \dot{x}_{t,0}, y_{t,0}, \dot{y}_{t,0}]^{\mathrm{T}}$ and $\lambda_\theta \triangleq P_{\mathrm{FA}}/C_\theta$. Then the following bearing LLR can be obtained:

$$\phi_{1:K}\left(\hat{\theta}_{1:K} \left| X_{t,0}^{1:4}\right.\right) = \sum_{i=1}^{n}\sum_{k=1}^{K} \ln\left[(1-P_{\mathrm{D}}) + \frac{P_{\mathrm{D}}}{\lambda_\theta} p_1\left(\hat{\theta}_{k,j}^{i}\right)\right] \tag{45}$$

$$p_1\left(\hat{\theta}_{k,j}^{i}\right) = \frac{1}{\sqrt{2\pi}\hat{\sigma}_{\theta,k}^{i}} \sum_{j=1}^{m_k^i} \exp\left(-\frac{1}{2}\frac{\left(\theta_{k,j}^{i} - \hat{\theta}_{k|k-1}^{i}\right)^2}{\left(\hat{\sigma}_{\theta,k}^{i}\right)^2}\right). \tag{46}$$

Assume that $\hat{X}_{t,0}^{1:4}$ maximizes (45), i.e.,

$$\hat{X}_{t,0}^{1:4} = \underset{X_{t,0}^{1:4}}{\operatorname{argmax}}\, \phi_{1:K}\left(\hat{\theta}_{1:K} \left| X_{t,0}^{1:4}\right.\right). \tag{47}$$

Note that (47) gives the kinematic component of the global optimal value $\hat{X}_{t,0}$ in (26). Then it can be used as a parameter to optimize the total LLR (43) as follows:

$$\begin{aligned}&\phi_{1:K}\left(\hat{Z}_{1:K} \left| \hat{X}_{t,0}^{1:4}, f\right.\right)\\ &\quad= \sum_{i=1}^{n}\sum_{k=1}^{K} \ln\left[(1-P_{\mathrm{D}}) + \frac{P_{\mathrm{D}}}{\lambda} p_1\left(\hat{z}_{k,j}^{i}\right)\right].\end{aligned} \tag{48}$$

Then the frequency component can be estimated by solving (48) as

$$\hat{f} = \underset{f}{\operatorname{argmax}}\, \phi_{1:K}\left(\hat{Z}_{1:K} \left| \hat{X}_{t,0}^{1:4}, f\right.\right). \tag{49}$$

The initial target state is then given by

$$\hat{X}_{t,0}^{\mathrm{guess}} = \left[\left(\hat{X}_{t,0}^{1:4}\right)^{\mathrm{T}}, \hat{f}\right]^{\mathrm{T}}, \tag{50}$$

which will be used by a gradient-based method to get the final global optimization $\hat{X}_{t,0}$. The rationale for the two-step rough grid-based method can be intuitively explained from the physical meaning of the estimate. With the ML-PDA method, an unbiased estimate of the target state can be obtained, and the expectation of the estimate equals the true target state [4]. When the DSF measurement is not available, we can only estimate the kinematic component from the bearing-only measurement. Theoretically, the bearing LLR takes its maximum value at the true state $X_{t,0}^{1:4}$. When the DSF measurement is available, the whole target state can be estimated by optimizing the total LLR. Theoretically, the total LLR achieves its maximum value at the true state $X_{t,0} = [(X_{t,0}^{1:4})^{\mathrm{T}}, f]^{\mathrm{T}}$. In other words, the expectation of $\hat{X}_{t,0}^{1:4}$ from optimizing the bearing LLR equals that from optimizing the total LLR. Consequently, we can first optimize the kinematic component with the bearing LLR and then optimize the frequency component with the total LLR. A rigorous mathematical justification is not available at this stage.

Assuming that each dimension of the target state space is divided into n_g cells, the computational complexity of the grid-based search for (26) is $O(n_g^5)$, and that for (47) and (49) becomes $O(n_g^4 + n_g)$. That is, the two-step rough grid-based method proposed here is an order of magnitude more computationally efficient than the direct rough grid-based search method.

If the sensor location is exactly known, the maximum of the LLR gives the candidate track estimate, which is then either validated as a true track or rejected as false by a track acceptance test [6]. However, when the sensor location is unknown—due to the fact that the LLR is evaluated using the estimated value of the sensor state $\hat{X}_{s,k}^{i}$ and not the true value $X_{s,k}^{i}$—the maximum of the LLR may not give the correct target state estimate. Accurate target state estimation depends on a more accurate LLR function or a more accurate sensor location. As in simultaneous location and mapping, the sensor (landmark) location is independent of the target (robot) trajectory [13]. The estimated target trajectory can be used to update the sensor location. Thus, the problem is converted into one of tracking multiple sensors using a mobile target track, which will be discussed in the next subsection.

B. Update Stage

Assume that the target initial state estimate in the prediction stage is denoted as $\hat{X}_{t,0}$. For the ith sensor, the target state at time k can be estimated as $\hat{X}_{t,k}$ by (1). Let

the ith sensor prediction state at time k be $\hat{X}^i_{s,k|k-1}$ with covariance matrix $P^i_{s,k|k-1}$, and let the target-originated measurement be predicted as $\hat{z}^i_{k|k-1}$ with the MMC $\hat{R}^i_k$—see (39) and (40). Then a fusion measurement innovation $\tilde{z}^i_k$ could be calculated by the PDA algorithm [14] and be used to update the ith sensor state. That is,

$$\tilde{z}^i_k = \sum_{z^{i,*}_{k,j}\in\hat{\Omega}^i_{g,k}} \omega^i_{k,j}\tilde{z}^{i,*}_{k,j} = \sum_{z^{i,*}_{k,j}\in\hat{\Omega}^i_{g,k}} \omega^i_{k,j}\left(z^{i,*}_{k,j} - \hat{z}^i_{k|k-1}\right) \quad (51)$$

$$\omega^i_{k,j} = \frac{\exp\left\{-\left(\tilde{z}^{i,*}_{k,j}\right)^{\mathrm{T}}\left(\hat{R}^i_k\right)^{-1}\left(\tilde{z}^{i,*}_{k,j}\right)\Big/2\right\}}{\varphi + \sum_{z^{i,*}_{k,j}\in\hat{\Omega}^i_{g,k}}\exp\left\{-\left(\tilde{z}^{i,*}_{k,j}\right)^{\mathrm{T}}\left(\hat{R}^i_k\right)^{-1}\left(\tilde{z}^{i,*}_{k,j}\right)\Big/2\right\}}, \quad (52)$$

where $\varphi = (2\pi)^{d_z/2}\lambda|\hat{R}^i_k|^{1/2}(1 - P_{\mathrm{D}}P_{\mathrm{G}})/P_{\mathrm{D}}$ and P_{G} is the probability that the target-originated measurement, if detected, lies within the gate [14]. Then a CKF algorithm is used to estimate the sensor state, given by (35)–(40) and (53)–(58). Calculate the cross-covariance matrix as

$$P^i_{xz,k|k-1} = \sum_{\eta=1}^{2d_s}\omega_\eta X^i_{s,k|k-1,\eta}\left(z^i_{k|k-1,\eta}\right)^{\mathrm{T}} - \hat{X}^i_{s,k|k-1}\left(\hat{z}^i_{k|k-1}\right)^{\mathrm{T}} \quad (53)$$

and the Kalman gain as

$$W^i_k = P^i_{xz,k|k-1}\left(\hat{R}^i_k\right)^{-1}. \quad (54)$$

Then update the sensor state and the corresponding error covariance using

$$\hat{X}^i_{s,k} = \hat{X}^i_{s,k|k-1} + W^i_k\tilde{z}^i_k \quad (55)$$

$$P^i_{s,k} = P^i_{s,k|k-1} - \left(1-\omega^i_{k,0}\right)W^i_k\hat{R}^i_k\left(W^i_k\right)^{\mathrm{T}} + W^i_kA^i_k\left(W^i_k\right)^{\mathrm{T}}, \quad (56)$$

where

$$\omega^i_{k,0} = \frac{\varphi}{\varphi + \sum_{z^{i,*}_{k,j}\in\hat{\Omega}^i_{g,k}}\exp\left\{-\left(\tilde{z}^{i,*}_{k,j}\right)^{\mathrm{T}}\left(\hat{R}^i_k\right)^{-1}\left(\tilde{z}^{i,*}_{k,j}\right)\Big/2\right\}} \quad (57)$$

$$A^i_k = \sum_{z^{i,*}_{k,j}\in\hat{\Omega}^i_{g,k}}\omega^i_{k,j}\left(\tilde{z}^{i,*}_{k,j}\right)\left(\tilde{z}^{i,*}_{k,j}\right)^{\mathrm{T}} - \left(\tilde{z}^i_k\right)\left(\tilde{z}^i_k\right)^{\mathrm{T}}. \quad (58)$$

To avoid any numerical instability in factorizing the sensor state covariance matrix (35) due to the sensor location uncertainty, a square-root version of the CKF can be adopted [1].

Through updating the sensor state and its covariance matrix, a more accurate and reliable sensor location can be obtained. This in turn helps to produce a more accurate LLR and track estimate in the next iteration. The pseudocode for the IML-PDA algorithm is presented in Algorithm 1.

Algorithm 1 IML-PDA Pseudocode

procedure $\{\bar{X}^i_{s,0}, P^i_{s,0}, Z_k\} \to \hat{X}_{t,0}, i = 1, \ldots, n, k = 1, \ldots, K$
Initialization: Let $\hat{X}^{i,(1)}_{s,0} = \bar{X}^i_{s,0}$, $P^{i,(1)}_{s,0} = P^i_{s,0}, p = 1$.
Iteration: While $(1 \le p \le I_{\max})$, do
    Prediction Stage
    {If $p = 1$, predict $\hat{X}^{i,(p)}_{s,k|k-1}$, $P^{i,(p)}_{s,k|k-1}$, $\hat{R}^{i,(p)}_k$ with $\hat{X}^{i,(1)}_{s,0}$, $P^{i,(1)}_{s,0}$; else with $\hat{X}^{i,(p-1)}_{s,k-1}$, $P^{i,(p-1)}_{s,k-1}$, see (28), (29), and (40).
    Establish the modified LLR $\phi^{(p)}_{1:K}(\hat{Z}_{1:K}|X_{t,0})$ with $\hat{X}^{i,(p)}_{s,k|k-1}$, $P^{i,(p)}_{s,k|k-1}$, $\hat{R}^{i,(p)}_k$, see (43).
    Optimize $\hat{X}^{(p)}_{t,0} = \underset{X_{t,0}}{\operatorname{argmax}}\left[\phi^{(p)}_{1:K}(\hat{Z}_{1:K}|X_{t,0})\right]$, see (47) and (49).}
    Update Stage
    {Calculate the fusion measurement innovation $\tilde{z}^{i,(p)}_k$ with $\hat{X}^{(p)}_{t,0}$, $\hat{X}^{i,(p)}_{s,k|k-1}$, $P^{i,(p)}_{s,k|k-1}$, see (51).
    Update $\hat{X}^{i,(p)}_{s,k}$, $P^{i,(p)}_{s,k}$ with $\hat{X}^{i,(p)}_{s,k|k-1}$, $P^{i,(p)}_{s,k|k-1}$, $\tilde{z}^{i,(p)}_k$, see (55) and (56).}
Estimation: $\hat{X}^{(p)}_{t,0} \to \hat{X}_{t,0}$.
End

VI. TRACK ACCEPTANCE TEST

In this section, a track-acceptance test method with sensor location uncertainty is presented. A binary-hypothesis test is constructed to test if the estimated track is acceptable or not. Consider the following two hypotheses: (1) There is one track with $X_{t,0}$ as the global optimum (H_1); (2) there is no track (H_0).

According to the Neyman–Pearson lemma [5, 26, 36], the most powerful test of H_0 against H_1 would be to compare the LLR global maximum at the track estimate to a threshold. The threshold value ϵ is selected to maximize the true-track detection probability P_{DT} at a given false-track acceptance probability P_{FT} [6], i.e.,

$$\epsilon = F^{-1}_\alpha(1 - P_{\mathrm{FT}}), \quad (59)$$

where $\alpha = \max\{\phi_{1:K}(\hat{Z}_{1:K}|X_{t,0})|\mathrm{H}_0\}$ is the LLR global maximum under H_0 and $F_\alpha(\alpha)$ represents the cumulative density function (cdf) of α. According to the extreme value theory [8, 15], the cdf $F_\alpha(\alpha)$ can be approximated by the following Gumbel function [6]:

$$F_\alpha(\alpha) = \exp\{-\exp[-a_n(\alpha - u_n)]\}, \quad (60)$$

where a_n and u_n are the scale and location parameters of the cdf, respectively. Also, one can derive the corresponding pdf $f_\alpha(\alpha)$ from $F_\alpha(\alpha)$ by finding the differential [32] as

$$f_\alpha(\alpha) = a_n\exp\{-a_n(\alpha - u_n) - \exp[-a_n(\alpha - u_n)]\}. \quad (61)$$

In order to estimate the Gumbel parameters a_n and u_n, an off-line method and a real-time method are presented in [6]. The former method can yield an optimal estimate in the ML sense at the cost of extensive Monte Carlo simulations. The latter method can estimate the Gumbel parameters in real time with less accuracy. Further, [31, 32] develop an accurate and real-time method to estimate the Gumbel parameter for the ML probabilistic multihypothesis tracker. In this paper, the off-line method

is invoked to estimate the Gumbel parameters a_n and u_n and to calculate the track acceptance threshold.

Denote the number of off-line Monte Carlo simulations as M_{off} and the LLR global maximum of the ith simulation under H_0 as α_i ($1 \le i \le M_{\text{off}}$). Then the parameters a_n and u_n can be estimated iteratively by the following equalities [6]:

$$\hat{a}_n = \left[\bar{\alpha} - \frac{\sum_{i=1}^{M_{\text{off}}} \alpha_i \exp\left(-\hat{a}_n \alpha_i\right)}{\sum_{i=1}^{M_{\text{off}}} \exp\left(-\hat{a}_n \alpha_i\right)} \right]^{-1} \tag{62}$$

$$\hat{u}_n = \frac{1}{\hat{a}_n} \left[\ln \frac{M_{\text{off}}}{\sum_{i=1}^{M_{\text{off}}} \exp\left(-\hat{a}_n \alpha_i\right)} \right], \tag{63}$$

where $\bar{\alpha} = \sum_{i=1}^{M_{\text{off}}} \alpha_i / M_{\text{off}}$. Thus, the threshold ϵ can be calculated from (59) for a given P_{FT}.

VII. PCRLB WITH SENSOR LOCATION UNCERTAINTY

Let $\hat{X}_{t,k}$ be an unbiased estimate of $X_{t,k}$ conditioned on the measurement set $Z_{1:k}$. Assume that the sensor state is estimated as $\hat{X}^i_{s,k}$ with the MMC matrix $\hat{R}^i_k = \text{diag}\{\hat{\sigma}^i_\theta, \hat{\sigma}^i_\gamma\}$. The PCRLB for the target state estimation error covariance matrix $P_{t,k}$ is defined to be the inverse of the Fisher information matrix J_k [35]. Thus,

$$P_{t,k} \triangleq E\left[\left(\hat{X}_{t,k} - X_{t,k}\right) \left(\hat{X}_{t,k} - X_{t,k}\right)^{\text{T}} \right] \ge J_k^{-1}. \tag{64}$$

Considering the linear dynamic system (1), the Fisher information matrix J_k is given recursively by [35]

$$J_{k+1} = \left(F_k J_k^{-1} F_k^{\text{T}}\right)^{-1} + J_{Z,k+1}. \tag{65}$$

The Fisher information matrix is initialized as $J_0 = P_{t,0}^{-1}$. The matrix $J_{Z,k+1}$ gives the measurement model's contributions to the PCRLB. Under the assumption that the sensors are mutually independent, the following can be obtained:

$$J_{Z,k} = \sum_{i=1}^{n} J^i_{Z,k}. \tag{66}$$

When there is measurement origin uncertainty and sensor location uncertainty, $J^i_{Z,k}$ is given by

$$J^i_{Z,k} = q^i_{2,k} \left[\frac{\left(\partial \hat{h}^i_k\right)^{\text{T}}}{\partial \hat{X}_{t,k}} \right] \left(\hat{R}^i_k\right)^{-1} \left[\frac{\left(\partial \hat{h}^i_k\right)^{\text{T}}}{\partial \hat{X}_{t,k}} \right]^{\text{T}}, \tag{67}$$

where $q^i_{2,k} \triangleq q^i_{2,k}(P_{\text{D}}, g, \lambda \hat{V}^i_{g,k})$ is the IRF, which depends on the detection probability, the gate parameter, and the expected number of false alarms in the validation gate [37, 38]. A detailed derivation of $q^i_{2,k}$ with sensor location uncertainty is presented in the Appendix. When the sensor location uncertainty is taken into account and incorporated into the MMC, the IRF becomes variable even if the detection probability is constant. If there is no sensor location uncertainty, $q^i_{2,k}(P_{\text{D}}, g, \lambda \hat{V}^i_{g,k}) = q_2(P_{\text{D}}, g, \lambda V_g) = q_2$. Thus, the modified PCRLB reduces to the conventional one [27].

In a sliding-window batch-type ML-PDA framework, there is no prior information about the initial target state. This means that (65) reduces to $J_k = J_{Z,k}$. Considering that the initial target state in each sliding window is estimated by the cumulative measurement set, the final PCRLB for the initial target state is given as follows—see (88):

$$\begin{aligned} J &= \sum_{k=1}^{K} J_{Z,k} = \sum_{k=1}^{K} \sum_{i=1}^{n} J^i_{Z,k} \\ &= \sum_{k=1}^{K} \sum_{i=1}^{n} q^i_{2,k} \left[\frac{\left(\partial \hat{h}^i_k\right)^{\text{T}}}{\partial \hat{X}_{t,k}} \right] \left(\hat{R}^i_k\right)^{-1} \left[\frac{\left(\partial \hat{h}^i_k\right)^{\text{T}}}{\partial \hat{X}_{t,k}} \right]^{\text{T}}. \end{aligned} \tag{68}$$

Note that the IRF values can be tabulated off-line before tracking, since they depend on the expected number of false alarms in the validation gates and not on the target and the sensor state. This makes it computationally efficient for real-time tracking and sensor-management applications.

VIII. SIMULATIONS

In simulations, the proposed algorithm is implemented for the track initialization of a constant-velocity target from multiple drifting asynchronous narrowband sonobuoys in heavy clutter. To illustrate its performance, simulations are carried out with three different objectives. First, the IML-PDA method is verified under hypothesis H_1 as well as under hypothesis H_0. Second, the proposed method is compared with the traditional techniques introduced in Section IV. Third, the effects of scenario parameters on the performance of the IML-PDA are analyzed.

The scenario parameters are given as follows. The frequency cell size is $C_\gamma = 0.25$ Hz, and the bearing cell size is $C_\theta = 3^\circ$. Under the assumption of uniform distribution in a cell, the frequency and bearing standard deviations are $\sigma_\gamma = 0.0722$ Hz and $\sigma_\theta = 0.866^\circ$, respectively. The SNR in a cell is $\text{SNR}_{\text{C}} = 6$ dB, the detection probability is $P_{\text{D}} = 0.6$, and the false-alarm probability is $P_{\text{FA}} = 0.028$. Then we can calculate the expected number of false alarms per unit volume as $\lambda \approx 0.037$. The validation gate parameter is $g = 5$. To validate the estimated track, the significance level is chosen as $P_{\text{FT}} = 5\%$. Also, 100 Monte Carlo runs are used.

There are eight operational sensors in the surveillance region. Their initial state means are given as follows (in kilometers): $\bar{X}^1_{s,0} = [1, 3]^{\text{T}}$, $\bar{X}^2_{s,0} = [1.6, 4]^{\text{T}}$, $\bar{X}^3_{s,0} = [1.8, 2.5]^{\text{T}}$, $\bar{X}^4_{s,0} = [2.3, 3.6]^{\text{T}}$, $\bar{X}^5_{s,0} = [2.9, 1.5]^{\text{T}}$, $\bar{X}^6_{s,0} = [3.2, 3.6]^{\text{T}}$, $\bar{X}^7_{s,0} = [4.5, 1]^{\text{T}}$, and $\bar{X}^8_{s,0} = [4, 2.7]^{\text{T}}$. All sensors move along with the ocean current at a velocity of $v_{\text{s}} = [1 \text{ m/s}, 1 \text{ m/s}]^{\text{T}}$, and their motions are disturbed by a zero-mean white Gaussian acceleration noise with standard deviation $\sigma_a = 0.05$ m/s^2. Thus, the uncertainty level in drifting motion is quantified by the process-noise covariance $Q_{\text{s}} = \sigma_v^2 = (0.5\sigma_a \Delta^2)^2$, where $\Delta = 30$ s is the sampling interval. The uncertainty level in the initial sensor location is quantified by the deployment

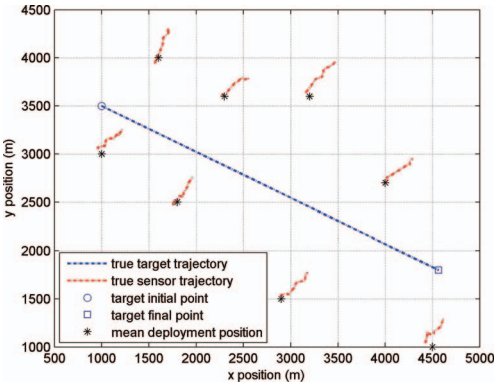

Fig. 2. True target trajectory.

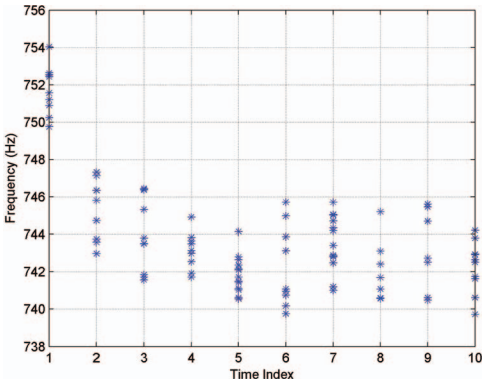

Fig. 5. DSF measurements of first sensor.

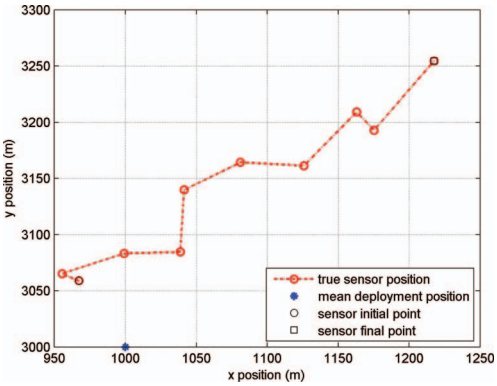

Fig. 3. First sensor's uncertain location.

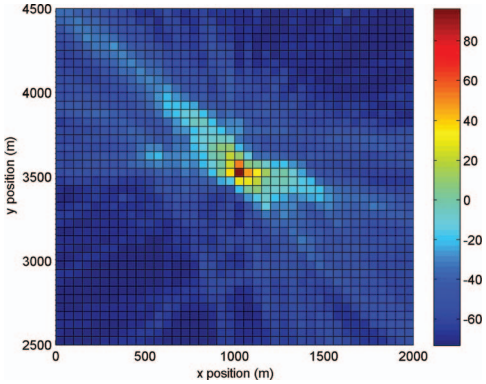

Fig. 6. LLR surface by X_s and R.

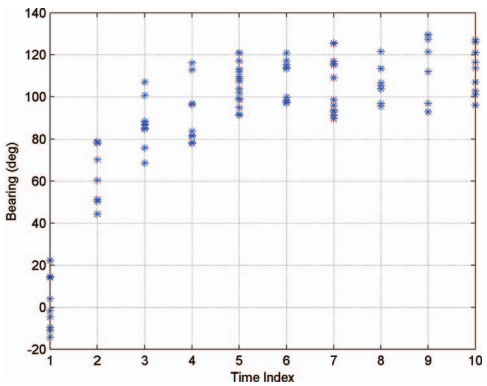

Fig. 4. Bearing measurements of first sensor.

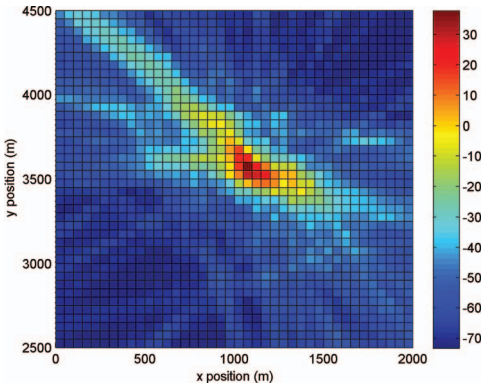

Fig. 7. LLR surface by $\bar{X}_s$ and R.

standard deviation $\sigma_p = 50$ m, i.e., the deployment covariance $P_{s,0} = \text{diag}\{\sigma_p^2, \sigma_p^2\}$. To simulate the asynchronous mode, the initial measurement time is assumed to be uniformly distributed and drawn from $[0, \Delta]$. When a target appears in the scenario, its initial state is $X_{t,0} = [1\text{ km}, 13.2\text{ m/s}, 3.5\text{ km}, -6.3\text{ m/s}, 750\text{ Hz}]^{\text{T}}$. The surveillance duration is 300 s, i.e., $K = 10$.

Fig. 2 shows the scenario including the true target trajectory, the sensor's drifting motion, and the initial and final points of the target trajectory. Fig. 3 shows the deployment uncertainty and the drifting uncertainty of the first sensor. Figs. 4 and 5 present the sets of bearing and DSF measurements, respectively, from the first sensor in one run. For simplicity, the field of view of the sensors is $[-20^\circ, 20^\circ] \times [-3\text{ Hz}, 3\text{ Hz}]$ centered on a target-originated measurement. Thus the volume of the surveillance region of each sensor is $V = 240$, and the number of false alarms in each sensor per frame follows a Poisson distribution with parameter $\lambda V \approx 8.958$.

To illustrate the effect of sensor location uncertainty on the LLR, three local LLR surfaces (from the top view) in one run are plotted. The LLR calculated with the true sensor locations and original measurement covariance is shown in Fig. 6. The LLR calculated with the sensor's deployment mean and original measurement covariance is shown in Fig. 7. The LLR calculated with the sensor's deployment mean with MMC (without iteration) is shown in Fig. 8. It can be seen from Fig. 6 that the maximum LLR

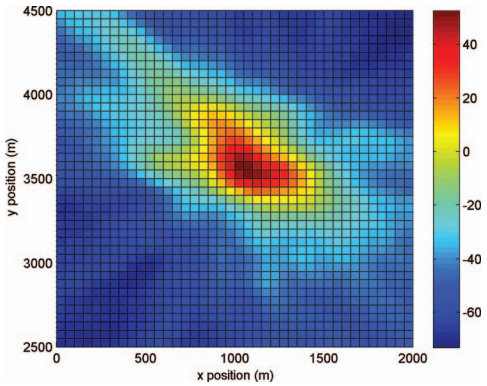

Fig. 8. LLR surface by $\bar{X}_s$ and $\hat{R}$.

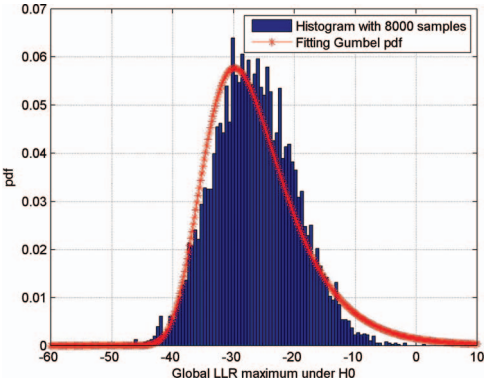

Fig. 9. Histogram and best-fitting Gumbel pdf.

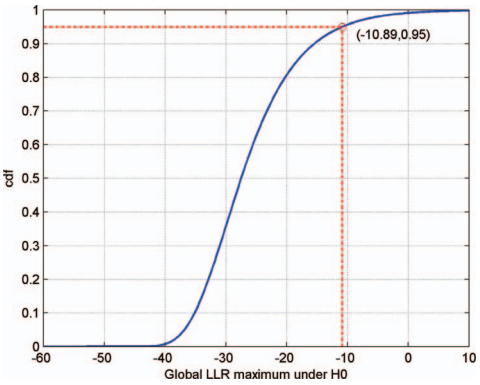

Fig. 10. Gumbel cdf and threshold.

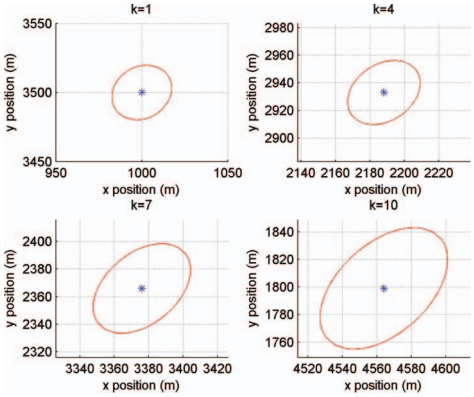

Fig. 11. 95% confidence ellipses at different instants.

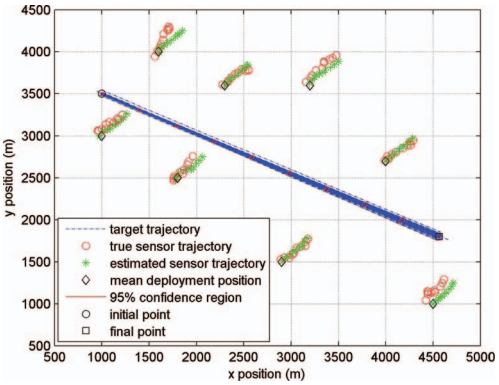

Fig. 12. Estimated target trajectory over 100 runs.

value corresponds to the true target position. However, the maximum values in Figs. 7 and 8 are not necessarily at the true target position. Unlike the sharp peak around the true target position in Fig. 6, the LLR surfaces in Figs. 7 and 8 have diffused peaks. Meanwhile, it can be noted that the LLR surface in Fig. 8 is flatter and smoother than that in Fig. 7, which helps to reach the larger LLR value at the true target position. In addition, there are many ridges and local maximum values in these LLR surfaces, which make the global optimization problem more complicated.

The maximum iteration number of IML-PDA in our simulation is $I_{\max} = 2$. Even with two iterations, our method reaches the PCRLB; thus, no further iterations are necessary. In order to calculate the threshold ϵ for the track acceptance test, off-line Monte Carlo simulations under H_0 are implemented to estimate the best-fitting parameters of the Gumbel distribution. Fig. 9 shows the histogram of the LLR global maxima with 8000 samples and plots the best-fitting Gumbel pdf curve. Fig. 10 illustrates the corresponding cdf curve and the threshold $\epsilon = -10.89$ with the significance level $P_{\text{FT}} = 0.05$. Fig. 11 shows the 95% confidence regions of the position estimates at different sampling instants ($k = 1$, 4, 7, and 10) based on the PCRLB. Being a batch parameter estimator, the ML-PDA uses all measurements in the window to estimate the parameters at the beginning of the window. From this estimate, subsequent estimates are obtained through open-loop prediction (i.e., without any additional measurements), which degrades the estimates at the end of the window. Similarly, the PCRLB is obtained at the beginning of the window and then propagated open loop, which inflates the PCRLB at subsequent times. See equations (3.7.4-12) and (3.7.4-13) in [4].

Fig. 12 shows the tracks formed from the estimates (dashed lines) and eight operational sensor trajectories (stars) in 100 Monte Carlo runs. All estimated tracks are accepted as valid tracks with the threshold ϵ. It can be seen that in 92 runs the estimated trajectory endpoints fall in the corresponding 95% uncertainty ellipses. When no target exists in the surveillance region, in two runs the estimated LLR global maxima exceed the threshold and

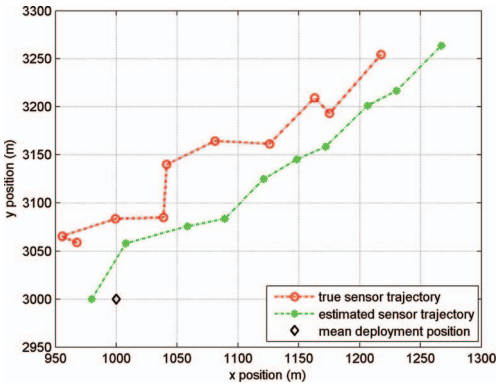

Fig. 13. Estimated sensor location.

TABLE I
Results of 100 Monte Carlo Runs ($I_{\max} = 2$)

Unit	$X_{t,0}$	$X_{t,0}^{\text{init}}$	$\bar{X}_{t,0}$	σ_{PCRLB}	$\bar{\sigma}$
Meters	1000	0 to 2000	1000.38	8.344	10.739
Meters per second	13.2	9 to 17	13.20	0.035	0.049
Meters	3500	2500 to 4500	3500.67	6.788	8.574
Meters per second	−6.3	−10 to −2	−6.28	0.069	0.076
Hertz	750	746 to 754	749.99	0.016	0.018

the corresponding tracks are wrongly accepted. Fig. 13 gives the estimated first sensor location in one run.

Table I shows the numerical results from 100 Monte Carlo runs. Here, $\bar{X}_{t,0}$ is the average of estimates, $\bar{\sigma}$ the sample variance of the estimates evaluated from 100 runs, and σ_{PCRLB} the theoretical PCRLB. The range of initial guesses used by the rough grid search are denoted as $X_{t,0}^{\text{init}}$. The efficiency of the estimator was verified using the normalized estimation error squared (NEES) [4, 23]. Assuming approximately Gaussian error, the NEES is chi-square distributed with d_t degrees of freedom. For the accepted tracks, the NEES is obtained as 5.41, which lies within the 95% confidence region [4.39, 5.65].

The performance of the proposed IML-PDA algorithm is compared with those of the Taylor-series-based ML-PDA method [29] and the deterministic sampling-based ML-PDA method, i.e., the IML-PDA without iteration. The SA method is not adopted here due to its high computational complexity in optimization when $n = 8$. Table II shows the average elapsed times for a single run with sliding-window width $K = 10$, the corresponding track acceptance levels with $\epsilon = -10.89$, and the percentage of accepted tracks falling within the 95% confidence ellipse for different methods. The average elapsed time for the iterations to converge is 8.82 s, which is less than the sampling interval. The computational times are on a PC with an Intel Core i5-5200U CPU running at 2.20 GHz. The average of estimates, the sample variance, and the NEES for different methods are also compared. For the scenario in this simulation, only the proposed method yields acceptable NEES levels. The main reason is that the proposed method can find the sensor locations accurately and hence qualifies the LLR precisely, which

TABLE II
Performance Comparison for Different Methods ($K = 10$)

		TS-ML-PDA	DS-ML-PDA	IML-PDA ($I_{\max} = 2$)
Track acceptance level (%)		99	99	100
Tracks in 95% ellipse (%)		81	82	92
Average elapsed time (s)		4.46	5.18	8.82
$\bar{X}_{t,0}$	x (m)	1013.67	1007.21	1000.38
	$\dot{x}$ (m/s)	13.23	13.19	13.20
	y (m)	3494.05	3489.64	3500.67
	$\dot{y}$ (m/s)	−6.28	−6.33	−6.28
	f (Hz)	749.98	749.98	749.99
$\bar{\sigma}$	x (m)	13.114	13.753	10.739
	$\dot{x}$ (m/s)	0.082	0.058	0.049
	y (m)	13.322	12.920	8.574
	$\dot{y}$ (m/s)	0.089	0.097	0.076
	f (Hz)	0.034	0.027	0.018
	NEES	8.81	10.66	5.41

Note: TS-ML-PDA = Taylor-series-based ML-PDA; DS-ML-PDA = deterministic sampling-based ML-PDA.

TABLE III
Effects of Parameters on Tracking Performance

		Track acceptance with ϵ (%)	Tracks in 95% ellipse (%)
$\sigma_a = 0.05, K = 10$	$\sigma_p = 50$	100	92
	$\sigma_p = 100$	99	89
	$\sigma_p = 200$	93	69
$\sigma_p = 50, K = 10$	$\sigma_a = 0.05$	100	92
	$\sigma_a = 0.2$	99	87
	$\sigma_a = 0.5$	83	72
$\sigma_a = 0.05, \sigma_p = 50$	$K = 10$	100	92
	$K = 7$	96	88
	$K = 5$	87	78

leads to accurate target state estimation compared with other methods.

Next, the effects of deployment uncertainty σ_p, drifting uncertainty σ_a, and window width K on the tracking performance are also analyzed in simulations. Table III shows the track acceptance levels, the percentage of accepted tracks falling within the 95% confidence ellipse with different parameters. For simplicity, the units of parameters are omitted in Table III. In addition, 2000 off-line simulations are carried out to estimate the threshold approximately when $K = 7$ and $K = 5$. The corresponding results are $\epsilon = -0.74$ and $\epsilon = 2.70$, respectively.

From Table III, it can be seen that with the increase in sensor deployment uncertainty and drifting uncertainty, the tracking performance will degrade. In addition, the higher the number of frames used in the estimator, the lower the threshold under H_0 and the higher the LLR global maximum under H_1. Consequently, using more frames is beneficial in improving the track acceptance probability. Furthermore, when the sensor location is uncertain, the tracking performance depends not only on the sensor location uncertainty level (deployment and drifting) but also on the geometry between the sensor and

the target. The quantification of the effects of the geometry on observability needs to be studied further.

IX. CONCLUSION

In this paper, an IML-PDA algorithm was proposed to passively track a nonmaneuvering target in heavy clutter with sensor location uncertainty. Due to the sensor's unknown location, the maximum value of the LLR does not occur at the true target state. An iterative optimization procedure was used to estimate the target state as well as the sensor state. At every iteration, a deterministic sampling-based algorithm was invoked to predict and update the sensor state, and a two-step rough grid-search technique was used to reduce the computational complexity. The PCRLB and the track acceptance test with sensor location uncertainty were also derived. Simulation results showed that the proposed method improves the tracking performance in a computationally efficient manner. Passively tracking multiple targets with sensor location uncertainty will be studied in future work. In addition, the effect of the sensor location uncertainty and the geometry on tracking performance needs further study.

APPENDIX. DERIVATION OF THE IRF

Assume that $J^i_{Z,k}$ is the measurement contribution to the PCRLB. Then it is given by [37]

$$\begin{aligned} J^i_{Z,k} &= E\left[-\Delta^{X_{t,k}}_{X_{t,k}} \ln p\left(Z^i_k \left| X_{t,k}\right.\right)\right] \\ &= \sum_{m^i_k=1}^{\infty} p\left(m^i_k\right) E\left[-\Delta^{X_{t,k}}_{X_{t,k}} \ln p\left(Z^i_k \left| X_{t,k}\right.\right) \left| m^i_k\right.\right] \\ &= \sum_{m^i_k=1}^{\infty} p\left(m^i_k\right) E\left[-\Delta^{X_{t,k}}_{X_{t,k}} \ln p\left(Z^i_k \left| X_{t,k}\right., m^i_k\right)\right] \\ &= \sum_{m^i_k=1}^{\infty} \int_V \cdots \int_V p\left(m^i_k\right) E\left[-\Delta^{X_{t,k}}_{X_{t,k}} \ln p\left(Z^i_k \left| X_{t,k}\right., \ m^i_k\right)\right] \\ &\quad \times p\left(Z^i_k \left| X_{t,k}\right., m^i_k\right) dZ^i_k. \end{aligned} \tag{69}$$

Given the sensor state $\hat{X}^i_{s,k}$ with MMC matrix $\hat{R}^i_k = \mathrm{diag}\{\hat{\sigma}^i_{\theta,k}, \hat{\sigma}^i_{\gamma,k}\}$, the following formulas can be obtained from (12):

$$p\left(Z^i_k \left| X_{t,k}\right., \ m^i_k\right) = a + b \sum_{j=1}^{m^i_k} \zeta_1\left(\hat{z}^i_{k,j}\right) \tag{70}$$

$$\begin{aligned} &\frac{\partial p\left(Z^i_k \left| X_{t,k}\right., m^i_k\right)}{\partial X_{t,k}} \\ &= b \sum_{j=1}^{m^i_k} \zeta_1\left(\hat{z}^i_{k,j}\right) \left(\frac{\Delta\hat{\theta}^i_{k,j}}{\left(\hat{\sigma}^i_{\theta,k}\right)^2} \frac{\partial\hat{\theta}^i_k}{\partial X_{t,k}} + \frac{\Delta\hat{\gamma}^i_{k,j}}{\left(\hat{\sigma}^i_{\gamma,k}\right)^2} \frac{\partial\hat{\gamma}^i_k}{\partial X_{t,k}} \right), \end{aligned} \tag{71}$$

where

$$a = \frac{1-\varepsilon\left(m^i_k\right)}{V^{m^i_k}} \tag{72}$$

$$b = \frac{\varepsilon\left(m^i_k\right)}{m^i_k V^{m^i_k - 1}} \frac{1}{2\pi\hat{\sigma}^i_{\theta,k}\hat{\sigma}^i_{\gamma,k}} \tag{73}$$

$$\zeta_1\left(\hat{z}^i_{k,j}\right) = \exp\left(-\frac{1}{2} \left(\frac{\left(\Delta\hat{\theta}^i_{k,j}\right)^2}{\left(\hat{\sigma}^i_{\theta,k}\right)^2} + \frac{\left(\Delta\hat{\gamma}^i_{k,j}\right)^2}{\left(\hat{\sigma}^i_{\gamma,k}\right)^2} \right) \right). \tag{74}$$

Then

$$\begin{aligned} &-\Delta^{X_{t,k}}_{X_{t,k}} \ln p\left(Z^i_k \left| X_{t,k}\right., \ m^i_k\right) p\left(Z^i_k \left| X_{t,k}\right., \ m^i_k\right) \\ &= \frac{\frac{\partial p\left(Z^i_k \left| X_{t,k}, m^i_k\right.\right)}{\partial X_{t,k}} \frac{\partial p\left(Z^i_k \left| X_{t,k}, m^i_k\right.\right)}{\partial X_{t,k}}}{p\left(Z^i_k \left| X_{t,k}\right., \ m^i_k\right)}. \end{aligned} \tag{75}$$

As discussed in [27], far-out measurements will be accorded small weights. Thus, the measurements are restricted to a validation gate. Assume that there are $m^{i,*}_k$ detections in the validation region $\hat{\Omega}^i_{g,k}$ defined by (41). For brevity, the superscripts and subscripts i, k, $*$, and t are omitted in the following. Then

$$\begin{aligned} &\frac{\partial p\left(Z^i_k \left| X_{t,k}\right., m^i_k\right)}{\partial X_{t,k}} \\ &= b \sum_{j=1}^{m^i_k} \zeta_1\left(\hat{z}^i_{k,j}\right) \left(\frac{\Delta\hat{\theta}_j}{(\hat{\sigma}_\theta)^2} \frac{\partial\hat{\theta}}{\partial X} + \frac{\Delta\hat{\gamma}_j}{\left(\hat{\sigma}_\gamma\right)^2} \frac{\partial\hat{\gamma}}{\partial X} \right). \end{aligned} \tag{76}$$

Change the integral variables from $Z = [\theta_1, \gamma_1, \ldots \theta_m, \gamma_m]^{\mathrm{T}}$ to $\xi = [\xi_{11}, \xi_{12}, \ldots \xi_{m1}, \xi_{m2}]^{\mathrm{T}}$, where

$$\xi_{j1} = \left(\theta_j - \hat{\theta}\left(X\right)\right) \big/ \hat{\sigma}_\theta \tag{77}$$

$$\xi_{j2} = \left(\gamma_j - \hat{\gamma}\left(X\right)\right) \big/ \hat{\sigma}_\gamma, \tag{78}$$

to obtain

$$\begin{aligned} J^i_{Z,k} = -\sum_{m=1}^{\infty} \int_{C_g} \cdots \int_{C_g} p\left(m\right) \left(\hat{\sigma}_\theta\hat{\sigma}_\gamma\right)^m \left[\frac{\partial p\left(\xi \left| X, m_k\right.\right)}{\partial X}\right] \\ \times \left[\frac{\partial p\left(\xi \left| X, m_k\right.\right)}{\partial X}\right]^{\mathrm{T}} \frac{1}{p\left(\xi \left| X, m_k\right.\right)} d\xi, \end{aligned} \tag{79}$$

where C_g is the circle of radius g. Because of the symmetry of the integration domain, the cross-terms vanish [19]. Thus,

$$\begin{aligned} J^i_{Z,k} = \sum_{m=1}^{\infty} p\left(m\right) \left(\hat{\sigma}_\theta\hat{\sigma}_\gamma\right)^m \\ \times \int_{C_g} \cdots \int_{C_g} \frac{b \sum_{j=1}^{m} \exp\left[-\xi^2_{j1} - \xi^2_{j2}\right] \Psi_j}{a/b + \sum_{j=1}^{m} \exp\left[-\frac{1}{2}\xi^2_{j1} - \frac{1}{2}\xi^2_{j2}\right]} d\xi \end{aligned} \tag{80}$$

$$\Psi_j = \frac{\xi^2_{j1}}{\hat{\sigma}^2_\theta} \left[\frac{\partial\hat{\theta}}{\partial X}\right] \left[\frac{\partial\hat{\theta}}{\partial X}\right]^{\mathrm{T}} + \frac{\xi^2_{j2}}{\hat{\sigma}^2_\gamma} \left[\frac{\partial\hat{\gamma}}{\partial X}\right] \left[\frac{\partial\hat{\gamma}}{\partial X}\right]^{\mathrm{T}}. \tag{81}$$

Using the symmetry of the integration domain again, we have

$$\begin{aligned}
&\int_{C_g}\cdots\int_{C_g}\frac{b\sum_{j=1}^{m}\exp\left[-\xi_{j1}^2-\xi_{j2}^2\right]\xi_{j2}^2}{a/b+\sum_{j=1}^{m}\exp\left[-\tfrac{1}{2}\xi_{j1}^2-\tfrac{1}{2}\xi_{j2}^2\right]}d\xi\\
&\quad=\int_{C_g}\cdots\int_{C_g}\frac{b\sum_{j=1}^{m}\exp\left[-\xi_{j1}^2-\xi_{j2}^2\right]\xi_{j1}^2}{a/b+\sum_{j=1}^{m}\exp\left[-\tfrac{1}{2}\xi_{j1}^2-\tfrac{1}{2}\xi_{j2}^2\right]}d\xi\\
&\quad=\sum_{j=1}^{m}\int_{C_g}\cdots\int_{C_g}\frac{b\exp\left[-\xi_{j1}^2-\xi_{j2}^2\right]\xi_{j1}^2}{a/b+\sum_{j=1}^{m}\exp\left[-\tfrac{1}{2}\xi_{j1}^2-\tfrac{1}{2}\xi_{j2}^2\right]}d\xi\\
&\quad=m\int_{C_g}\cdots\int_{C_g}\frac{b\exp\left[-\xi_{11}^2-\xi_{12}^2\right]\xi_{11}^2}{a/b+\sum_{j=1}^{m}\exp\left[-\tfrac{1}{2}\xi_{j1}^2-\tfrac{1}{2}\xi_{j2}^2\right]}d\xi.
\end{aligned}\tag{82}$$

Defining

$$\begin{aligned}
&q_1\left(m,P_{\mathrm{D}},g,\lambda\hat{V}_g\right)\\
&\quad=m\int_{C_g}\cdots\int_{C_g}\frac{b\exp\left[-\xi_{11}^2-\xi_{12}^2\right]\xi_{11}^2}{a/b+\sum_{j=1}^{m}\exp\left[-\tfrac{1}{2}\xi_{j1}^2-\tfrac{1}{2}\xi_{j2}^2\right]}d\xi
\end{aligned}\tag{83}$$

yields

$$\begin{aligned}
J_{Z,k}^{i}&=\sum_{m=1}^{\infty}p(m)\left(\hat{\sigma}_\theta\hat{\sigma}_\gamma\right)^m q_1(\cdot)\left\{\frac{1}{\hat{\sigma}_\theta^2}\left[\frac{\partial\hat{\theta}}{\partial X}\right]\left[\frac{\partial\hat{\theta}}{\partial X}\right]^{\mathrm{T}}\right.\\
&\quad\left.+\frac{1}{\hat{\sigma}_\gamma^2}\left[\frac{\partial\hat{\gamma}}{\partial X}\right]\left[\frac{\partial\hat{\gamma}}{\partial X}\right]^{\mathrm{T}}\right\}\\
&=\sum_{m=1}^{\infty}p(m)\left(\hat{\sigma}_\theta\hat{\sigma}_\gamma\right)^m q_1(\cdot)\left[\frac{\partial\hat{h}^{\mathrm{T}}}{\partial X}\right]R^{-1}\left[\frac{\partial\hat{h}^{\mathrm{T}}}{\partial X}\right]^{\mathrm{T}}.
\end{aligned}\tag{84}$$

Following [19], with a second change of variables from (ξ_{j1},ξ_{j2}) to (ρ_j,ω_j), the corresponding polar coordinates in $q_1(\cdot)$ yield

$$\begin{aligned}
q_1(\cdot)=\frac{m}{2}(2\pi)^m\int_0^g\cdots\int_0^g\frac{b\exp\left(-\rho_1^2\right)\rho_1^2\left(\rho_1\cdots\rho_m\right)}{a/b+\sum_{j=1}^{m}\exp\left(-\rho_j^2/2\right)}\\
\times d\rho_1\cdots d\rho_m.
\end{aligned}\tag{85}$$

Substitute a and b into (85) and $p(m)$ into (84) and denote

$$\begin{aligned}
&q_2\left(P_{\mathrm{D}},g,\lambda\hat{V}_g\right)\\
&=\sum_{m=1}^{\infty}\frac{P_{\mathrm{D}}u_f(m-1)2^{m-2}}{g^{2m-2}}\\
&\times\int_0^g\cdots\int_0^g\frac{\exp\left(-\rho_1^2\right)\rho_1^2\left(\rho_1\cdots\rho_m\right)}{\frac{1-P_{\mathrm{D}}}{P_{\mathrm{D}}}\frac{2\lambda\hat{V}_g}{g^2}+\sum_{j=1}^{m}\exp\left(-\rho_j^2/2\right)}d\rho_1\cdots d\rho_m.
\end{aligned}\tag{86}$$

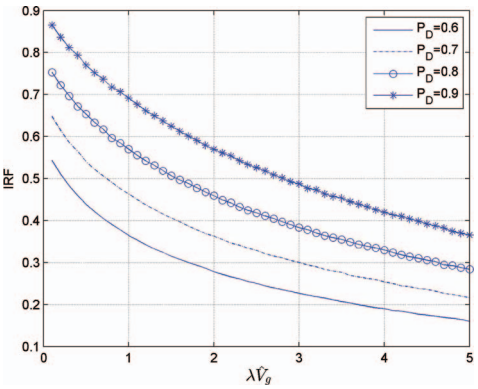

Fig. 14. IRF curves versus P_{D} and $\lambda\hat{V}_g$.

Finally,

$$J_{Z,k}^{i}=q_2\left(P_{\mathrm{D}},g,\lambda\hat{V}_g\right)\cdot\left[\frac{\partial\hat{h}^{\mathrm{T}}}{\partial X}\right]R^{-1}\left[\frac{\partial\hat{h}^{\mathrm{T}}}{\partial X}\right]^{\mathrm{T}}.\tag{87}$$

Reintroducing all the subscripts and superscripts, we have

$$\begin{aligned}
J_{Z,k}&=\sum_{i=1}^{n}q_{2,k}^{i}\left(P_{\mathrm{D}},g,\lambda\hat{V}_{g,k}^{i}\right)\\
&\quad\cdot\left[\frac{\partial\left(\hat{h}_k^i\right)^{\mathrm{T}}}{\partial X_{t,k}}\right]\left[\hat{R}_k^i\right]^{-1}\left[\frac{\partial\left(\hat{h}_k^i\right)^{\mathrm{T}}}{\partial X_{t,k}}\right]^{\mathrm{T}}.
\end{aligned}\tag{88}$$

Fig. 14 shows the IRF $q_{2,k}^{i}(P_{\mathrm{D}},g,\lambda\hat{V}_{g,k}^{i})$ values with respect to different detection probabilities P_{D} and validation volumes $\hat{V}_{g,k}^{i}$ multiplied by λ.

REFERENCES

[1] Arasaratnam, I., and Haykin, S.
Cubature Kalman filters.
IEEE Transactions on Automatic Control, **54**, 6 (2009), 1254–1269.

[2] Bailey, T., and Durrant-Whyte, H.
Simultaneous localization and mapping (SLAM): Part II.
IEEE Robotics & Automation Magazine, **13**, 3 (Sept. 2006), 108–117.

[3] Bar-Shalom, Y., and Li, X. R.
Multitarget-Multisensor Tracking: Principles and Techniques.
Storrs, CT: YBS Publishing, 1995.

[4] Bar-Shalom, Y., Li, X. R., and Kirubarajan, T.
Estimation with Applications to Tracking and Navigation.
New York: Wiley, 2001.

[5] Barra, J.-R.
Mathematical Basis of Statistics (L. Herbach, Trans.).
New York: Academic Press, 1981.

[6] Blanding, W. R., Willett, P. K., and Bar-Shalom, Y.
Offline and real-time methods for ML-PDA track validation.
IEEE Transactions on Signal Processing, **55**, 5 (May 2007), 1994–2006.

[7] Blanding, W. R., Willett, P. K., Bar-Shalom, Y., and Lynch, R. S.
Directed subspace search ML-PDA with application to active sonar tracking.
IEEE Transactions on Aerospace and Electronic Systems, **44**, 1 (Jan. 2008), 201–216.

[8] Castillo, E.
Extreme Value Theory in Engineering.
Boston: Academic Press, 1988.

[9] Chan, Y. T., and Jardine, F. L.
Target localization and tracking from Doppler-shift measurements.
IEEE Journal of Oceanic Engineering, **15**, 3 (July 1990), 251–257.

[10] Chan, Y. T., and Towers, J. J.
Passive localization from Doppler-shifted frequency measurements.
IEEE Transactions on Signal Processing, **40**, 10 (Oct. 1992), 2594–2598.

[11] Clark, J. M. C., Vinter, R. B., and Yaqoob, M. M.
Shifted Rayleigh filter: A new algorithm for bearings-only tracking.
IEEE Transactions on Aerospace and Electronic Systems, **43**, 4 (Oct. 2007), 1373–1384.

[12] Daum, F.
Nonlinear filters: Beyond the Kalman filter.
IEEE Aerospace and Electronic Systems Magazine, **20**, 8 (Aug. 2005), 57–69.

[13] Durrant-Whyte, H., and Bailey, T.
Simultaneous localization and mapping: Part I.
IEEE Robotics & Automation Magazine, **13**, 2 (June 2006), 99–110.

[14] Fortmann, T., Bar-Shalom, Y., and Scheffe, M.
Sonar tracking of multiple targets using joint probabilistic data association.
IEEE Journal of Oceanic Engineering, **8**, 3 (July 1983), 173–184.

[15] Gumbel, E. J.
Statistics of Extremes.
New York: Columbia University Press, 1958.

[16] Hernandez, M. L., Kirubarajan, T., and Bar-Shalom, Y.
Multisensor resource deployment using posterior Cramér–Rao bounds.
IEEE Transactions on Aerospace and Electronic Systems, **40**, 2 (Apr. 2004), 399–416.

[17] Hillis, D. B.
Using a genetic algorithm for multi-hypothesis tracking.
In *Ninth IEEE International Conference on Tools with Artificial Intelligence*,
Newport Beach, CA, Nov. 1997, 112–117.

[18] Ho, K. C., Lu, X., and Kovavisaruch, L.
Source localization using TDOA and FDOA measurements in the presence of receiver location errors: Analysis and solution.
IEEE Transactions on Signal Processing, **55**, 2 (Feb. 2007), 684–696.

[19] Jauffret, C., and Bar-Shalom, Y.
Track formation with bearing and frequency measurements in clutter.
IEEE Transactions on Aerospace and Electronic Systems, **26**, 6 (Nov. 1990), 999–1010.

[20] Jiang, X., Harishan, K., Tharmarasa, R., Kirubarajan, T., and Thayaparan, T.
Integrated track initialization and maintenance in heavy clutter using probabilistic data association.
Signal Processing, **94** (Jan. 2014), 241–250.

[21] Julier, S. J., and Uhlmann, J. K.
Unscented filtering and nonlinear estimation.
Proceedings of the IEEE, **92**, 3 (Mar. 2004), 401–422.

[22] Karan, M., Wang, J., and Hammel, S. E.
Bearings-only tracking with sea trial sonar data from multiple asynchronous sonobuoys.
In *Undersea Defence Technology*, Sydney, Australia, Feb. 1998.

[23] Kirubarajan, T., and Bar-Shalom, Y.
Low observable target motion analysis using amplitude information.
IEEE Transactions on Aerospace and Electronic Systems, **32**, 4 (Oct. 1996), 1367–1384.

[24] Kronhamn, T. R.
Bearings-only target motion analysis based on a multihypothesis Kalman filter and adaptive ownship motion control.
IEE Proceedings–Radar, Sonar and Navigation, **145**, 4 (Aug. 1998), 247–252.

[25] Marrs, A. D.
Asynchronous multi-sensor tracking in clutter with uncertain sensor locations using Bayesian sequential Monte Carlo methods.
In *Aerospace Conference*, Big Sky, MT, Mar. 2001, **5**, 2171–2178.

[26] Neyman, J., and Pearson, E. S.
On the problem of the most efficient tests of statistical hypotheses.
Philosophical Transactions of the Royal Society of London, Series A, **231A** (1933), 289–338.

[27] Niu, R., Willett, P., and Bar-Shalom, Y.
Matrix CRLB scaling due to measurements of uncertain origin.
IEEE Transactions on Signal Processing, **49**, 7 (July 2001), 1325–1335.

[28] Peach, N.
Bearings-only tracking using a set of range-parameterised extended Kalman filters.
IEE Proceedings–Control Theory and Applications, **142**, 1 (Jan. 1995), 73–80.

[29] Punithakumar, K., Kirubarajan, T., and Hernandez, M.
Multisensor deployment using PCRLBs, incorporating sensor deployment and motion uncertainties.
IEEE Transactions on Aerospace and Electronic Systems, **42**, 4 (Oct. 2006), 1474–1485.

[30] Ristic, B., and Arulampalam, M. S.
Tracking a manoeuvring target using angle-only measurements: Algorithms and performance.
Signal Processing, **83**, 6 (June 2003), 1223–1238.

[31] Schoenecker, S., Luginbuhl, T., Willett, P., and Bar-Shalom, Y.
Extreme-value analysis for ML-PMHT, part 2: Target trackability.
IEEE Transactions on Aerospace and Electronic Systems, **50**, 4 (Oct. 2014), 2515–2527.

[32] Schoenecker, S., Willett, P., and Bar-Shalom, Y.
Extreme-value analysis for ML-PMHT, part 1: Threshold determination.
IEEE Transactions on Aerospace and Electronic Systems, **50**, 4 (Oct. 2014), 2500–2514.

[33] Tharmarasa, R., Kirubarajan, T., and Hernandez, M.
Large-scale optimal sensor array management for multitarget tracking.
IEEE Transactions on Systems, Man, and Cybernetics, Part C: Applications and Reviews, **37**, 5 (Sept. 2007), 803–814.

[34] Tharmarasa, R., Lang, T., and Kirubarajan, T.
Tracking with poorly localized sensors in multistatic sensor networks.
Proceedings of SPIE, **6969** (Apr. 2008), 69690P.

[35] Tichavsky, P., Muravchik, C. H., and Nehorai, A.
Posterior Cramér–Rao bounds for discrete-time nonlinear filtering.
IEEE Transactions on Signal Processing, **46**, 5 (May 1998), 1386–1396.

[36] Van Trees, H. L.
Detection, Estimation, and Modulation Theory.
New York: John Wiley & Sons, 2004.

[37] Zhang, X., and Willett, P. K.

Cramér–Rao bounds for discrete time linear filtering with measurement origin uncertainty.
In *Proceedings of the Workshop on Estimation, Tracking and Fusion: A Tribute to Yaakov Bar-Shalom*, Monterey, CA, May 2001, 546–561.

[38] Zhang, X., Willett, P. K., and Bar-Shalom, Y.
Dynamic Cramér–Rao bound for target tracking in clutter.
IEEE Transactions on Aerospace and Electronic Systems, **41**, 4 (Oct. 2005), 1154–1167.

Yunfei Guo was born in China in 1978. He received a B.S. degree in electrical engineering from Yanshan University, China, in 2002, and a Ph.D. degree in electrical engineering from Zhejiang University, China, in 2007. From 2014 to 2015 he was a visiting professor in the Department of Electrical and Computer Engineering at McMaster University, Canada. Currently, he is an associate professor in the Automation School at Hangzhou Dianzi University, Hangzhou, Zhejiang, China. He is also serving as the deputy secretary general at the China Information Fusion Society. His research interests are in estimation, target detection, target tracking, and multisource information fusion.

Ratnasingham Tharmarasa was born in Sri Lanka in 1975. He received a B.Sc.Eng. degree in electronic and telecommunication engineering from the University of Moratuwa, Sri Lanka, in 2001, and M.A.Sc. and Ph.D. degrees in electrical engineering from McMaster University, Canada, in 2003 and 2007, respectively. From 2001 to 2002 he was an instructor in electronic and telecommunication engineering at the University of Moratuwa. During 2002–2007 he was a graduate student and research assistant in the Department of Electrical and Computer Engineering at McMaster University, Canada, where he is currently working as a research associate. His research interests include target tracking, information fusion, and sensor resource management.

Sreeraman Rajan (M'90—SM'06) received a B.E. degree in electronics and communications from Bharathiyar University, Coimbatore, India, in 1987; an M.Sc. degree in electrical engineering from Tulane University, New Orleans, LA, in 1992; and a Ph.D. degree in electrical engineering from the University of New Brunswick, Fredericton, Canada, in 2004.

From 1986 to 1990 he was a scientific officer with the Reactor Control Division, Bhabha Atomic Research Center, Bombay, India, after undergoing an intense training in nuclear science and engineering from its training school. At the center, he developed systems for control, safety, and regulation of nuclear research and power reactors. During 1997 and 1998 he carried out research under a grant from Siemens Corporate Research, Princeton, NJ. From 1999 to 2000 he was with JDS Uniphase, Ottawa, Canada, where he worked on optical components and the development of signal-processing algorithms for advanced fiber-optic modules. From 2000 to 2003 he was with Ceyba Corporation, Ottawa, Canada, where he developed channel monitoring, dynamic equalization, and optical power-control solutions for advanced ultralong-haul and long-haul fiber-optic communication systems. In 2004 he was with Biopeak Corporation, where he developed signal-processing algorithms for noninvasive medical devices. From December 2004 to June 2015 he was a defense scientist with Defence Research and Development Canada, Ottawa, Canada. In July 2015 he joined Carleton University as a Canadian research chair (Tier II) in sensors systems in its Department of Systems and Computer Engineering. Since 2010 he has also been an adjunct professor at the School of Electrical Engineering and Computer Science, University of Ottawa, Canada, and since June 2015 an adjunct professor in the Department of Electrical and Computer Engineering, Royal Military College, Kingston, Ontario, Canada. He is the holder of one patent and two disclosures of invention. He is an author of 90 journal articles and conference papers. His research interests include signal processing, biomedical signal processing, communication, and pattern classification.

He is currently the IEEE Canada Area East Chair and Chair of the IEEE Ottawa EMBS Chapter. He was awarded the IEEE MGA Achievement Award in 2012 and recognized for his IEEE contributions with the Queen Elizabeth II Diamond Jubilee Medal in 2012. He has been involved in organizing several IEEE conferences and has been a reviewer for several IEEE journals and conferences.

Taek Lyul Song (M'83) was born in Andong, Korea, in 1952. He received a B.Sc. degree in nuclear engineering from Seoul National University, Seoul, South Korea, in 1974, and M.Sc. and Ph.D. degrees in aerospace engineering from the University of Texas at Austin, in 1981 and 1983, respectively. From 1974 to 1994 he was with the Agency for Defense Development, where his major research topics included missile guidance and control and control systems design, target tracking, and navigation systems analysis. He has been a professor in the Electronic Systems Engineering Department, Hanyang University, since 1995. His research interests include target state estimation, guidance, navigation, and control.

Thiagalingam Kirubarajan (S'95—M'98—SM'03) was born in Sri Lanka in 1969. He received B.A. and M.A. degrees in electrical and information engineering from Cambridge University, England, in 1991 and 1993, respectively, and M.S. and Ph.D. degrees in electrical engineering from the University of Connecticut, Storrs, in 1995 and 1998. Currently he is a distinguished engineering professor in the Electrical and Computer Engineering Department at McMaster University, Hamilton, Ontario, Canada. He is also the Canada research chair in information fusion, and is serving as an adjunct assistant professor and the associate director of the Estimation and Signal Processing Research Laboratory at the University of Connecticut. His research interests are in estimation, target tracking, multisource information fusion, sensor resource management, signal detection and fault diagnosis. His research activities at McMaster University and at the University of Connecticut are supported by U.S. Missile Defense Agency, U.S. Office of Naval Research, NASA, Qualtech Systems, Inc., Raytheon Canada Ltd., and Defense Research Development Canada, Ottawa. In September 2001 he served in a DARPA expert panel on unattended surveillance, homeland defense, and counterterrorism. He has also served as a consultant in these areas to a number of companies, including Motorola Corporation, Northrop Grumman Corporation, Pacific-Sierra Research Corporation, Lockheed Martin Corporation, Qualtech Systems, Inc., Orincon Corporation, and BAE Systems. He has worked on the development of a number of engineering software programs, including BEARDAT for target localization from bearing and frequency measurements in clutter, and FUSEDAT for fusion of multisensor data for tracking. He has also worked with Qualtech Systems, Inc., to develop an advanced fault-diagnosis engine. He has published more than 110 articles in the areas of his research interests, in addition to one book on estimation, tracking, and navigation and two edited volumes. Dr. Kirubarajan is a recipient of the Ontario Premier's Research Excellence Award (2002).